

Haverford College

Haverford Scholarship

Faculty Publications

Astronomy

2020

The HI morphology and stellar properties of strongly barred galaxies: support for bar quenching in massive spirals

L. Newnham

Kelley M. Hess

Karen Masters

Haverford College, klmasters@haverford.edu

Sandor Kruk

Samantha J. Penny







Follow this and additional works at: https://scholarship.haverford.edu/astronomy_facpubs

Repository Citation

Newnham, L, Hess, KM, Masters, KL, Kruk, S, Penny, SJ, et al. (2020). The HI morphology and stellar properties of strongly barred galaxies: support for bar quenching in massive spirals. *Monthly Notices of the Royal Astronomical Society* 492(4): 4697-4715

This Journal Article is brought to you for free and open access by the Astronomy at Haverford Scholarship. It has been accepted for inclusion in Faculty Publications by an authorized administrator of Haverford Scholarship. For more information, please contact nmedeiro@haverford.edu.

The H I morphology and stellar properties of strongly barred galaxies: support for bar quenching in massive spirals

L. Newnham ¹★, Kelley M. Hess,^{2,3} Karen L. Masters ^{1,4}, Sandor Kruk ⁵†, Samantha J. Penny ¹, Tim Lingard ¹ and R. J. Smethurst ⁶

¹*Institute of Cosmology and Gravitation, University of Portsmouth, Dennis Sciama Building, Portsmouth PO1 3FX, UK*

²*Kapteyn Astronomical Institute, University of Groningen, Landleven 12, NL-9747 AD Groningen, the Netherlands*

³*ASTRON, the Netherlands Institute for Radio Astronomy, Postbus 2, NL-7990 AA Dwingeloo, the Netherlands*

⁴*Department of Physics and Astronomy, Haverford College, 370 Lancaster Ave, Haverford, PA 19041, USA*

⁵*European Space Agency, ESTEC, Keplerlaan 1, PO Box 299, NL-2200 AG Noordwijk, the Netherlands*

⁶*Oxford Astrophysics, Denys Wilkinson Building, Keble Road, Oxford OX1 3RH, UK*

Accepted 2020 January 6. Received 2020 January 3; in original form 2019 January 4

ABSTRACT

Galactic bars are able to affect the evolution of galaxies by redistributing their gas, possibly contributing to the cessation of star formation. Several recent works point to ‘bar quenching’ playing an important role in massive disc galaxies. We construct a sample of six gas-rich and strongly barred disc galaxies with resolved H I observations. This sample of galaxies, which we call H I-rich barred galaxies, was identified with the help of Galaxy Zoo to find galaxies hosting a strong bar, and the Arecibo Legacy Fast Arecibo L-band Feed Array blind H I survey to identify galaxies with a high H I content. The combination of strong bar and high gas fraction is rare, so this set of six galaxies is the largest sample of its type with resolved H I observations. We measure the gas fractions, H I morphology and kinematics, and use archival optical data from the Sloan Digital Sky Survey to reveal star formation histories and bar properties. The galaxies with the lowest gas fractions (still very high for their mass) show clear H I holes, dynamically advanced bars, and low star formation rates, while those with the highest gas fractions show little impact from their bar on the H I morphology, and are still actively star-forming. These galaxies support a picture in which the movement of gas by bars can lead to star formation quenching. How these unusual galaxies came to be is an open question.

Key words: galaxies: evolution – galaxies: general – galaxies: kinematics and dynamics – galaxies: spiral – galaxies: star formation – galaxies: structure.

1 INTRODUCTION

Within a galaxy, a bar is a structure in the central region made up of stars, gas, and dust following elongated orbits. Bars are found in 30–70 percent of disc galaxies within $0.01 < z < 0.1$ (e.g. Menéndez-Delmestre et al. 2007; Barazza, Jogee & Marinova 2008; Nair & Abraham 2010a; Masters et al. 2011). A stellar bar has been demonstrated to disrupt and influence the motion of the material in the central region of its galaxy (Pfenniger & Norman 1990; Regan, Sheth & Vogel 1999), as well as having an impact on the spiral arms (Schwarz 1984; Hart et al. 2018); these impacts have been seen in many simulations (Ostriker & Peebles 1973; Hohl

1976; Athanassoula 2002; Martel, Kawata & Ellison 2013; Fanali et al. 2015; Carles et al. 2016; Spinoso et al. 2017; Khoperskov et al. 2018), and are thought to affect the disc galaxy’s overall evolution (Kormendy & Kennicutt 2004; Athanassoula 2013). Since this process is slow, it is one of the processes of so-called ‘secular’ (or slow) evolution of galaxies.

The formation of a bar is not a certainty in disc galaxies; after all not all spiral galaxies host bars [Nair & Abraham 2010a; Masters et al. 2011; a fact which even today is discussed as a puzzle as numerical simulations almost ubiquitously form them (Saha & Elmegreen 2018; Sellwood, Shen & Li 2019)]. The time it takes to develop a bar is thought to vary depending on a variety of dynamical factors in a galaxy, such as the ratio of stellar mass to halo mass, the gas content, rotational velocity, etc. (e.g. for an extensive discussion see Athanassoula 2013). Once the bar has formed, it will continue to grow in length and width with age, however simulations

* E-mail: lucy.newnham@port.ac.uk

† ESA Research Fellow.

demonstrate that the correlation between the age of a bar and its length is not linear in a given galaxy, nor is the relation the same between different galaxies (e.g. Athanassoula 2013). Thus, we cannot assume the age of a bar by looking at its physical length, or the length with respect to the diameter of the stellar disc, even though longer bars are likely to be dynamically older.

Many studies have investigated which galaxies are more likely to have bars. In the largest recent studies, it was observed that disc galaxies that have a larger mass and are redder in colour are the most common hosts of bars (e.g. Nair & Abraham 2010a; Masters et al. 2011; Cervantes Sodi 2017). This correlation suggests that bars form around the time a galaxy ceases to be star forming and is making the transition from the blue cloud to the red sequence. However, in Nair & Abraham (2010b), the distribution is actually double peaked, with more bars in both low-mass and the highest mass galaxies. It has also been observed that late-type disc galaxies which have no bulge or at least a low bulge-to-total luminosity ratio are more likely to host a bar (Barazza et al. 2008), and other results suggest no strong correlations with colour or mass (Erwin 2018). These results may initially appear contradictory, but depend on details such as how the disc galaxies were selected (i.e. if redder spirals are excluded by a colour selection), how bars are identified, and whether strong and weak bars are included. There are several methods used to define the strength of a bar, including, but not limited to, the bar–interbar contrast ratio (Elmegreen et al. 1996), the axial ratio and bar length (Martin 1995; Martinet & Friedli 1997; Chapelon, Contini & Davoust 1999), and the ratio of the flux inside the bar to the flux outside (not including the bulge) (Rozas, Knapen & Beckman 1998). There is more information on this in Section 3.1.1.

It has been observed that an increasing bar fraction in a galaxy population coincides with the increase in the average time since the start of star formation quenching (Masters et al. 2011; Skibba et al. 2012; Smethurst et al. 2015), an observation which suggests bars have some responsibility for quenching within a galaxy. Additionally, there is evidence showing that through funnelling gas towards the centre, bars may be the cause of morphological quenching (Athanassoula 1992; Sheth et al. 2005; Masters et al. 2012; Cheung et al. 2013; Vera, Alonso & Coldwell 2016). There is even a suggestion this process may have been important in the Milky Way’s history (Haywood et al. 2016).

A galaxy’s environment has also been linked to its likelihood of developing a bar, with bars appearing more common in higher density regions (Skibba et al. 2012). These, presumably tidally induced bars, may form and grow earlier than expected (related to the stellar mass of the host galaxy; Noguchi 1988; Giuricin et al. 1993; Moore et al. 1996; Eskridge et al. 2000; Skibba et al. 2012). This is still debated, as some research finds no such link (van den Bergh 2002; Li et al. 2009; Marinova et al. 2012), and some studies find only a poor link (Lin et al. 2014).

There exists a clear trend between galaxies that host strong bars and the atomic gas content (Davoust & Contini 2004; Masters et al. 2012; Cervantes Sodi 2017). Using the global neutral hydrogen (HI) measurements made by the Arecibo Legacy Fast Arecibo L-band Feed Array (ALFALFA) Survey (Giovanelli et al. 2005; Haynes et al. 2011, 2018), Masters et al. (2012) found that galaxies hosting strong bars (identified with Galaxy Zoo as in Masters et al. 2011) are more likely to be gas-poor. Masters et al. (2012) also observed that galaxies that did not follow that trend, i.e. the ones that had a strong bar but were also gas-rich, were typically redder than similar gas-rich but non-barred galaxies, suggesting that star formation might have ceased earlier in those galaxies. Erwin (2018) suggests that this observation is caused by a redshift bias, with higher stellar

mass (less HI-rich) galaxies being observed only at larger distance where their bars may be more likely to be missed. However, Kruck et al. (2018) demonstrate that strong bars are identified reliably in galaxies across the entire redshift range in the method used by Masters et al. (2012). So the result is robust for strong bars.

Galaxies use their HI reserves to form stars (Leroy et al. 2008; Saintonge et al. 2011). In dense regions, and usually in the presence of dust, HI will form H₂ in molecular clouds, which then cool further, collapse, and forms new stars. Eventually, the HI will run out in the galaxy and star formation will cease. Star formation may also cease if the HI is unable to cool due to significant torque or other dynamical processes (e.g. bar torques, Tubbs 1982). The general picture that HI-rich galaxies are star forming holds well, with a clear correlation between star formation properties and HI content (e.g. Saintonge et al. 2012).

Numerical simulations of bar formation in disc galaxies can now realistically include a dissipative gas counterpart, and the effects of that on the galaxy. The formation of a bar in these is shown to aid the movement of material, with angular momentum being transported outwards and material transported in, towards the centre, in the inner bar regions (Bournaud & Combes 2002). The gas is especially influenced by this since it is dynamically cold and responds more easily to gravitational perturbations (e.g. as explored in Athanassoula 2013).

Kraljic, Bournaud & Martig (2012), exploring zoomed-in cosmological simulations, and Athanassoula, Machado & Rodionov (2013), for an isolated galaxy, use detailed *N*-body and Smooth Particle Hydrodynamics (SPH) simulations to show the formation and growth of a bar with hydrodynamic models of gas flow, and present gas morphology as well as stars. In particular, Athanassoula et al. (2013) and Spinoso et al. (2017) predict the HI kinematics of strongly barred galaxies. In these simulations, the gas within the bar corotation radius (bar region) infalls to the very centre (inner kpc) where it enhances star formation. Gas outside of this region is also prevented from entering due to the bar, thereby creating a ‘hole’. This agrees extremely well with the THINGS observations of M95 (the only strongly barred galaxy in the sample, Walter et al. 2008), which show a large HI hole in the bar region. In this paper, we will further test the predictions of these simulations in a sample of strongly barred gas-rich galaxies.

We introduce a sample of galaxies which we call HI-rich barred (HIRB) galaxies. This study was initiated to help reveal the evolution of galaxies with strong bars and large quantities of neutral hydrogen (HI). As mentioned above, galaxies tend not to host a strong bar and have a large reserve of HI (Masters et al. 2012). This is likely because the presence of significant quantities of gas inhibits and slows bar formation (Villa-Vargas, Shlosman & Heller 2010; Athanassoula et al. 2013). The HIRB galaxies are unusual as they all host a strong bar and still have large reserves of HI, such that they would be considered HI-rich galaxies relative to typical scaling relations (Huang et al. 2012).

The paper is organized as follows: in Section 2, we discuss the data collected for this study, a description of the sample selection criteria, the available archival optical and spectroscopic data, and finally the resolved HI data collected for them by us using the VLA (NSF’s Karl G. Jansky Very Large Array¹) and the GMRT (the Giant Metrewave Radio Telescope in Pune, India). In Section 3,

¹The National Radio Astronomy Observatory is a facility of the National Science Foundation operated under cooperative agreement by Associated Universities, Inc.

we discuss the properties of the six HIRB galaxies revealed by these data. In Section 4, we compare our results to simulations, and provide a plausible physical picture of the galaxies. We conclude and summarize our results in Section 5. Where distances are needed to calculate physical lengths or other properties, we use $H_0 = 70 \text{ km s}^{-1} \text{ Mpc}^{-1}$ to convert from redshift.

2 DATA

2.1 Sample selection

We introduce here the HIRB galaxy sample. This sample has been designed to investigate a rare type of disc galaxy which are both strongly barred and very H I gas-rich. The parent sample consisted of 2090 non-edge-on disc galaxies [selected through the Sloan Digital Sky Survey (SDSS)], with H I gas content detections from the ALFALFA 40 per cent survey (which was the part of ALFALFA available at the time the HIRB galaxy survey was initiated; Haynes et al. 2011) and bar identifications from Galaxy Zoo (GZ2, Willett et al. 2013) that were the basis of the study published in Masters et al. (2012). This sample was built from a volume-limited subset of the Galaxy Zoo sample, with $0.01 < z < 0.05$ (in order to allow for reliable distance measurements and an adequate angular resolution to detect bars in the galaxies). The SDSS spectroscopic limiting magnitude of $r = 17.7$ corresponds to a volume-limited sample of galaxies with $M_r < -19.0$ out to $z = 0.05$.

For more details of the selection of the parent sample from Galaxy Zoo and ALFALFA see (Masters et al. 2012), we show in Fig. 1 H I gas fraction from ALFALFA (Haynes et al. 2011, 2018) against an estimate of the stellar mass, from K -correction fit to Petrosian magnitudes,² for the entire sample (grey points) with strongly barred galaxies highlighted in orange. The solid lines show the best-fitting relation for all (blue) and just strongly barred (orange) galaxies, while the dashed line is 3σ above this mean line. Our HIRB galaxies are shown by the large coloured numbers, and the rainbow colour and numerical order reveals a ranking by an increasing physical size of the bar (which we discuss later in Section 3.1.1).³

Using this large sample, we started by selecting objects which fit the criteria to be an HIRB galaxy, namely H I-rich and strongly barred. In Masters et al. (2012), it was shown that these are rare. We define the gas-rich sample to have a gas fraction, $\log(M_{\text{HI}}/M_*)$, greater than 3σ more than the mean value for their stellar mass as shown in Fig. 1. Masters et al. (2012) find that a small fraction of the entire parent sample meet both these criteria. These HIRB galaxies represent 17 per cent of galaxies with comparable H I mass for their stellar mass, i.e. the bar fraction of such H I-rich massive galaxies is just 17 per cent.

Since these strongly barred, gas-rich galaxies are rare, it is hard to find a large sample of them nearby. We have to go to larger volumes (and therefore higher redshifts) in order to have a reasonable sample. However, to be able to observe the H I at high enough resolution to resolve the bar region and with the column density sensitivity required to detect the disc requires tens of hours of observing for a single source at $z > 0.02$. Due to this we ended up observing just seven of the nearest and/or largest in angular size sources for a total of 118 h of telescope time on the GMRT and VLA combined.

² K -correction fit and filter transformations designed to work using SDSS spectroscopy and photometry are described in Blanton & Roweis (2007).

³This plot uses ALFALFA100, the initial search for HIRB galaxies used instead ALFALFA40 which was available at the time.

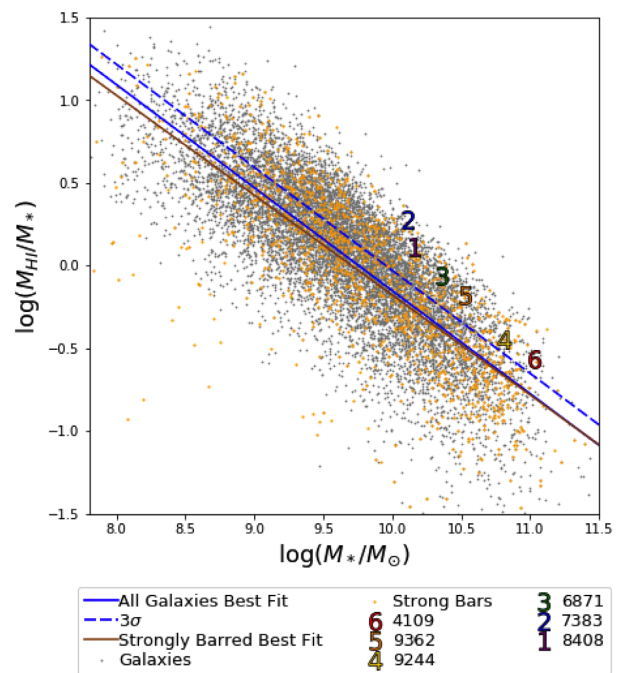


Figure 1. H I content (from ALFALFA; Haynes et al. 2018), expressed relative to the stellar mass versus the stellar mass of galaxies in our sample (See Section 2.1). A volume-limited subset of ALFALFA100 galaxies are plotted in grey and the orange points show all galaxies within that sample that host a strong bar ($p_{\text{bar}} > 0.5$). The blue line fits the trend between the H I mass fraction and the stellar mass, with the blue dashed line showing a trend 3σ more gas rich than that. The individually coloured numbers represent the six HIRB galaxies observed and detailed in this paper, and the rainbow colour and numerical order reveals an increasing absolute bar length (see Section 3.1.2).

These seven were selected from the small group for strongly barred and H I-rich galaxies discussed at the beginning of this section. From there we chose the galaxies with the largest angular size that displayed a range of optical colours and bulge sizes. The larger the angular size, the more likely we will be able to resolve detail. These galaxies happened to all have relatively large stellar mass ($\log(M_*/M_\odot) > 10.1$).

The properties of these seven galaxies are summarized in Table 1, where you can see they span a range of properties, while all being gas rich and strongly barred. SDSS optical gri images are shown for the final six in Fig. 2. Unfortunately, the data from one source were corrupted by a nearby continuum source (see Section 2.3 for details on the observing and data reduction).

Our HIRB galaxies share many properties with those in the (H I) HighMass Survey ongoing at the JVLA (Hallenbeck et al. 2014) in that they are unusually massive and gas-rich, so HighMass make good $z \sim 0$ analogues of the types of galaxies which will dominate detections in SKA surveys (as well as the similar H I mass and gas-rich galaxies in HIGHz at $z \sim 0.2$; Catinella & Cortese 2015). HighMass galaxies were selected without any reference to visual morphology, and there are no obvious strongly barred galaxies in that sample. The general conclusion from the five HighMass galaxies with resolved H I is that they must be galaxies about to transition from a gas-rich but relatively inactive state, to a state of vigorous star formation (Hallenbeck et al. 2014).

There are other ongoing surveys of H I-rich galaxies which are also relevant for comparison. The Bluediscs project (Wang et al.

Table 1. Properties of the seven HIRB galaxies used in sample selection. Columns: (1) Name of the Galaxy, (2) Right ascension and declination, (3) Redshift, (4) the debiased fraction of GZ users identifying a bar, (5) SDSS Petrosian stellar mass, (6) ALFALFA H I mass, (7) the global width from ALFALFA (Haynes et al. 2011), (8) Number and colour used to represent in plots. The data for galaxy UGC 5830 are not used in the main analysis, more information on this is given in Section 2.3.1.

Name	RA and Dec. (J2000)	z	p_{bar}	$\log(M_{\star}/M_{\odot})$	$\log(M_{\text{HI}}/M_{\odot})$	W50 km s^{-1}	Number and colour (8)
(1)	(2)	(3)	(4)	(5)	(6)	(7)	
UGC 5830	10 42 38.0 + 23 57 07	0.044	0.62	11.17	10.40	624	
UGC 4109	07 56 16.6 + 11 39 41	0.046	0.91	11.04	10.46	304	Red 6
UGC 9362	14 33 17.5 + 03 54 10	0.030	0.75	10.50	10.34	113	Orange 5
UGC 9244	14 26 08.4 + 05 14 15	0.028	0.59	10.94	10.36	414	Yellow 4
UGC 6871	11 53 46.3 + 10 24 10	0.022	0.54	10.55	10.29	346	Green 3
UGC 7383	12 20 01.3 + 08 36 26	0.025	0.58	10.10	10.38	294	Blue 2
UGC 8408	13 23 00.3 + 13 57 02	0.024	0.88	10.19	10.26	290	Purple 1

2013) is using Westerbork Synthesis Radio Telescope (WSRT) observations to investigate the reason for excess H I in some galaxies over that predicted from scaling relations, while Lemonias et al. (2014) present VLA C configuration observations of a sample of H I-rich, but not star-forming, spirals (including for UGC 4109 in our sample). Meanwhile, Lee et al. (2014)’s ‘H I Monsters’ survey is a CO survey of very H I-rich galaxies. None of these surveys use information on galaxy morphology for selection, nor comment on it in their results, while it is central to the HIRBs selection. In both Bluediscs and H I Monsters, they find that H I-rich (but not necessarily high H I fraction) spirals are simply scaled-up versions of lower mass spirals, and sit on all the typical scaling relations. The passive H I-rich spirals of Lemonias et al. (2014) however show more extended and lower surface brightness H I than is typical, and it is interesting to note that roughly half of them appear to host relatively strong bars (see their fig. 3; although we have not explored the significance of this fraction).

2.2 Optical photometry, spectra, and morphologies

All optical photometric and spectroscopic data used in this paper are taken from the final release of the first phase of the Sloan Digital Sky Survey (SDSS Data Release 7, Abazajian et al. 2009), and all HIRB galaxies (and their parent sample) are part of the Main Galaxy Sample of SDSS (MGS, Strauss et al. 2002).

We make use of morphologies from the second phase of Galaxy Zoo (GZ2, Willett et al. 2013). These come from the aggregation of classifications made by numerous volunteers on images from the SDSS for the brightest 25 per cent of MGS galaxies (those with $m_r < 17$). In GZ2, a median of 45 people was looking at each galaxy. The GZ2 classification process starts with the question: ‘Is this galaxy simply smooth and rounded, with no signs of a disc?’, where one of the options were ‘features or disc’, followed by ‘Could this be a disc viewed edge-on?’. The weighted and debiased fraction of users answering a specific way to a single question in GZ2 is denoted, p_x . The sample defined in Masters et al. (2012) used $p_{\text{features}} p_{\text{not edge-on}} > 0.25$. After these questions, the citizen scientists were asked ‘Is there a sign of a bar feature throughout the centre of the galaxy?’ From this we can get the probability of a galaxy having a bar. We call this p_{bar} and define this as the percentage of ‘yes’ votes to that question (although note that it is not exactly this, following a correction for redshift bias as described in Willett et al. 2013). For example, a galaxy with $p_{\text{bar}} = 0.5$ suggests that 50 per cent of the people asked if there is a visible bar responded ‘yes’. A comparison with other bar identifications is shown in appendix A of Masters et al. (2012,

and also see Willett et al. 2013; Kruk et al. 2018). Using this, $p_{\text{bar}} > 0.5$ is classified as a strong bar (SB), the definition used for the HIRB galaxies. As discussed above, the parent sample is a subset of the Galaxy Zoo 2 sample which overlaps with the ALFALFA 40 per cent footprint.

SDSS provided optical photometry in *ugriz*-bands, and with a variety of apertures. In the NASA Sloan Atlas, Blanton et al. (2005) provide matched aperture photometry also including NUV and FUV photometry from the *GALEX* satellite (Martin et al. 2005). We use the Absolute magnitude in rest-frame *GALEX*/SDSS *FNugriz*, from Petrosian apertures to generate colours, and the stellar mass from *K*-correction fit to Petrosian magnitudes. A colour–mass diagram is shown for the parent sample in Fig. 3, with the six HIRB galaxies highlighted with the large coloured numbers (in order of bar length). As is obvious from that diagram, HIRB galaxies span a range of optical colours.

The SDSS images can also be used to provide more quantitative details of the bar structures. Following the method described in Kruk et al. (2018), we obtained two- or three-component decompositions for each galaxy in the sample. This is particularly useful in providing bar lengths and bar position angles. We give more details on how bar lengths are obtained in Section 3.1.1 below.

We further make use of the SDSS fibre spectra to obtain measurements related to the stellar populations and ionized gas in these galaxies. We note that the SDSS fibre has a 3 arcsec size, which represents only 1.2–2.9 kpc at the distance of the HIRB galaxies, as such these spectra measure the properties of only the central parts of these galaxies, well within the bar radius. A full spectral fitting is beyond the scope of this work, however we make use of line fluxes and spectral index measurements provided by the Max Planck Institute for Astrophysics and John’s Hopkins University collaboration (MPA-JHU).⁴ These star formation rates are found using the technique described in Brinchmann et al. (2004) while updating the procedure for aperture corrections. This procedure included calculating the light outside the fibre per galaxy, then fitting stochastic models to the photometry, akin to those used in Salim et al. (2007).⁵

⁴<http://www.mpa-garching.mpg.de/SDSS/> The team made up of Stephane Charlot (IAP), Guinevere Kauffmann and Simon White (MPA), Tim Heckman (JHU), Christy Tremonti (Max-Planck for Astronomy, Heidelberg - formerly JHU) and Jarle Brinchmann (Sterrewach Leiden - formerly MPA).

⁵<https://www.mpa-garching.mpg.de/SDSS/DR7/sfrs.html>

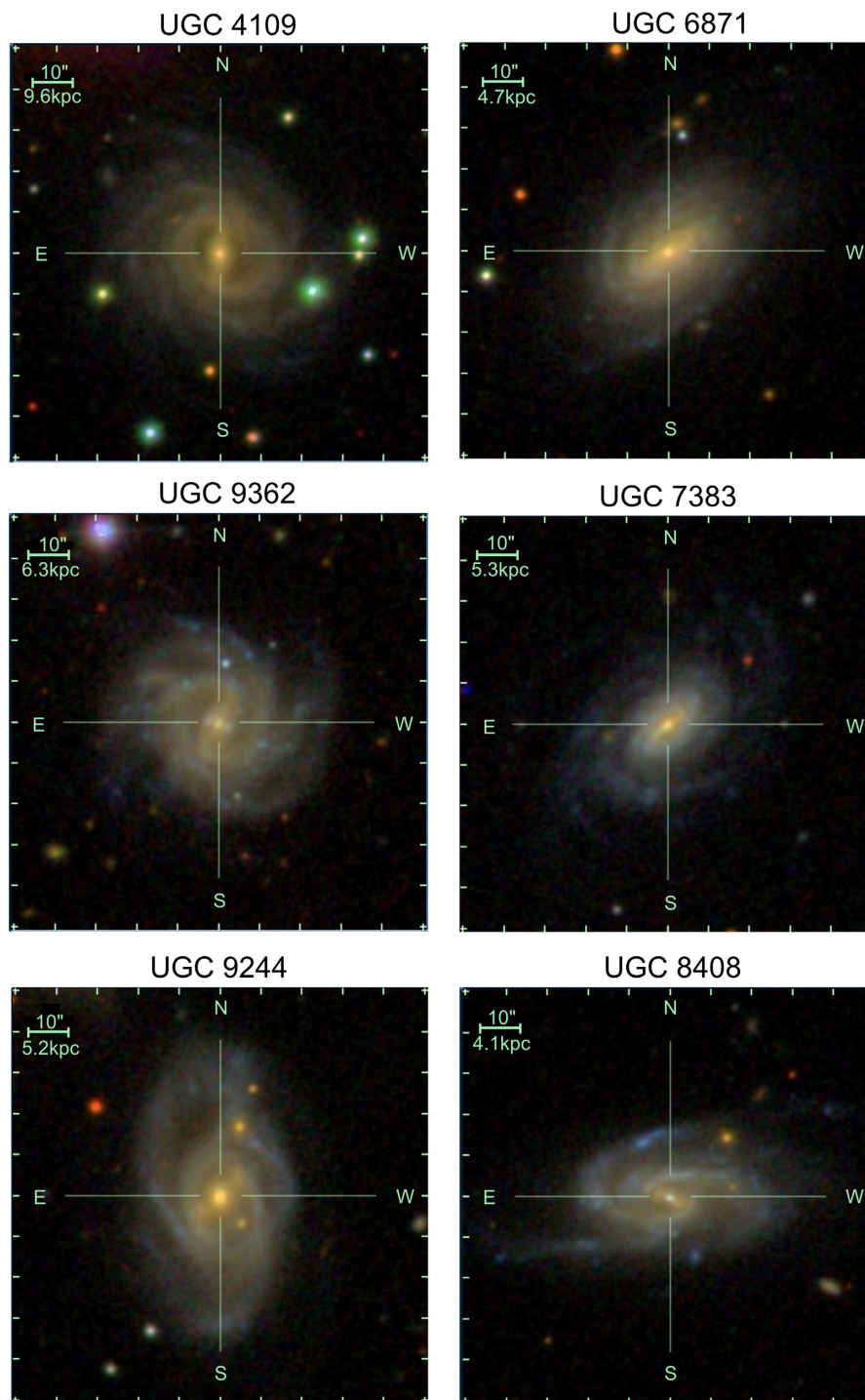


Figure 2. Optical SDSS gri images of each of the six galaxies in the HIRB sample.

2.3 Resolved H I data

Our H I observations were designed to resolve the optical bar at the centre of the galaxy in addition to the rest of the disc. However, the scarcity of gas-rich, strongly barred galaxies meant that the majority of our targets are at relatively large distances ($0.022 < z < 0.046$) compared to typical H I interferometric targets ($z < 0.02$). The small beam required to resolve the centres of these galaxies necessitated observing with the B-configuration of the VLA with its maximum baseline of 10 km. The GMRT is comprised of 30

antennas similarly arranged in a fixed ‘Y’-configuration with a maximum baseline of 25 km, but also has 14 antennas concentrated within 1 km. The combination of long baselines with a compact core mean that the performance of the GMRT is often compared to the VLA in B-configuration. In balancing resolution with column density sensitivity, our Galaxies were challenging targets to observe. In this section, we describe our observing, imaging, and source finding strategies. Table 2 summarizes the properties of the final data cubes for all six galaxies.

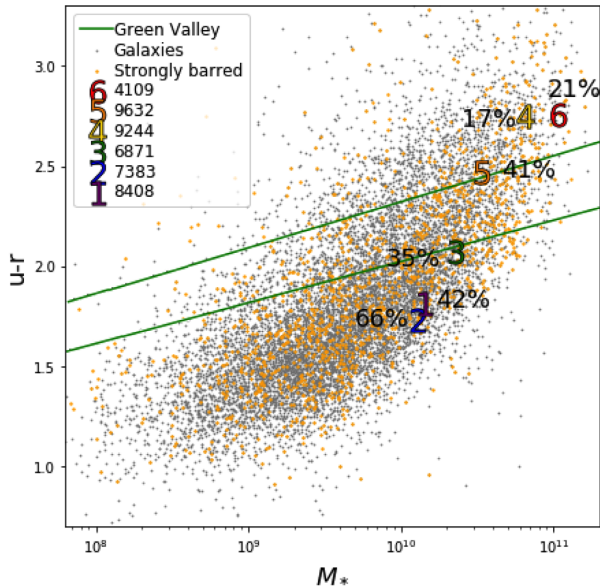


Figure 3. A colour–mass diagram showing the volume-limited ALFALFA100 galaxies (grey), those of which are strongly barred (orange) and with the HIRB galaxies highlighted with individual numbers and colours. Two of the HIRBs are at the high-mass end of the blue cloud, two are at opposing sides of the green valley (within the green lines; Schawinski et al. 2014), and the remaining two are in the red sequence. The percentage numbers adjacent to each HIRB galaxy display the gas fraction that galaxy has.

2.3.1 VLA data reduction

We observed UGC 5830, UGC 4109, UGC 6871, and UGC 7383 with the VLA in B-configuration between 2013 November and 2014 January (Project ID: 13B-142). Each observation was centred on the H I systemic velocity of the galaxy measured by ALFALFA. The bandwidth spanned 8 MHz divided into 512 channels, resulting in a 3.3 km s^{-1} resolution over approximately 1700 km s^{-1} . We observed each galaxy for $6 \times 2 \text{ h}$, including calibration, resulting in a total of 10 h on-source. The data were calibrated and imaged using standard methods in Common Astronomy Software Applications (CASA, McMullin et al. 2007). The final images were made with natural weighting to provide the best column density sensitivity.

We imaged each 2 hour observing session individually to inspect the quality of the data before combining all sessions together. However, UGC 7383 required special attention. Although we were able to image all the individual sessions and achieve the expected

rms, σ , for unknown reasons the CASA clean task was unable to properly combine the first session with the remaining five. Instead, we imaged the first session individually, the last five sessions together, and combined the two resulting cubes in the image plane, weighting them by $1/\sigma^2$ to create a final dirty (not yet cleaned) image cube of the full 10 h. We performed the same weighting combination procedure on the synthesized dirty beam cubes. In order to clean the dirty image cubes, we imported the data to the Astronomical Image Processing System (AIPS, Greisen 2003) and cleaned the channels individually using the AIPS task APCLN.

For UGC 5830, we realized after imaging that a source greater than 0.3 Jy lay at the half power point of the primary beam, causing significant difficulties for imaging and continuum subtraction. We attempted to do self-calibration on the field, and to subtract the continuum with a number of higher order polynomials, but could not completely remove the interfering continuum source. We concluded that ‘third generation’ calibration techniques – which include direction-dependent gain calibration – would be required, but given the faintness of H I profile from ALFALFA (UGC 5830 has the second highest redshift in our sample), the effort to make a reliable H I map outweighed the benefits. In the rest of the paper, we exclude UGC 5830 from the analysis.

Table 2 shows the details from these observations, including, but not limited to, the spatial resolution, the rms, and the H I column density.

2.3.2 GMRT data reduction

We observed UGC 9244, UGC 9362, UGC 8408 with the GMRT for 22–24 h each including calibration, with a total of approximately 18–19 h on-source. The observations took place in 2016 February–March and 2017 February, while the galaxies were up at night to avoid solar interference and to minimize the incidence of other ground-based radio frequency interference. We observed using the GMRT’s spectral zoom mode with 256 channels across 4 MHz bandwidth centred on the ALFALFA H I redshift of the galaxy. This provided 3.3 km s^{-1} spectral resolution over approximately 800 km s^{-1} . Unfortunately, due to roll-off at the edges of the sideband, less of the band was usable. In the worst case, combined with RFI, the final cube covered 460 km s^{-1} , which fortunately included the galaxy and a few channels for continuum subtraction.

We calibrated the data in the standard way using AIPS while on site at the GMRT. For imaging purposes the data were spectrally averaged as little as possible to be able to detect reliable signal in individual channels, while still resolving the motion of the gas

Table 2. Properties of the HIRB galaxy final data cubes. Columns: (1) Name of the Galaxy, (2) The spectral resolution of the final image, (3) Weighting applied to the data during reduction, (4) The rms of the final image, (5) The resolution of the restoring clean beam, (6) The H I column density, (7) The observatory used to collect the resolved H I data.

Galaxy Name (1)	Spectral resolution (km s^{-1}) (2)	Robustness (Weighting) (3)	rms ($\text{Jy beam}^{-1} \text{chan}^{-1}$) (4)	Resolution (arcsec) (5)	H I column density $\text{atoms cm}^{-2} \text{km s}^{-1}$ (6)	Observatory (7)
UGC 4109	19.8	natural	1.8×10^{-04}	8.9×5.1	1.1×10^{20}	VLA
UGC 9362	31.9	natural	8.0×10^{-05}	7.3×4.8	1.0×10^{20}	GMRT
UGC 9244	27.5	natural	2.3×10^{-04}	7.8×5.3	2.3×10^{20}	GMRT
UGC 6871	19.8	natural	3.1×10^{-04}	5.9×4.8	3.0×10^{20}	VLA
UGC 7383	9.9	smoothed	5.5×10^{-04}	10.1×8.2	1.8×10^{20}	VLA
UGC 8408	27.5	natural	2.1×10^{-04}	9.6×4.8	1.8×10^{20}	GMRT

in the disc. The galaxies were imaged with natural weighting to provide the best column density sensitivity as possible given the long baselines. In addition, UGC 9362 benefited from self-calibration in AIPS which reduced the noise in the final image by approximately 1/3.

Despite careful flagging, we found that there were still stripes in some of the images suggesting bad baselines which we had been unable to isolate from looking at the individual visibilities. Stripes in the image plane are equivalent to a high point in the UV plane, and its complex conjugate which has the same value. From the orientation and width of the stripes, we can predict the location of the high points in the UV plane. Thus, in order to eliminate the stripes for each galaxy, we Fourier transformed the image cube using the `fft` task in MIRIAD (Sault, Teuben & Wright 2011), blanked the outlier points in the resulting UV plane data cubes (each image cube produces an amplitude and phase cube), and performed the inverse Fourier transform to return to the image plane (The inverse also produces an amplitude and phase cube but the phases of sky image are zero everywhere.). In the end, we eliminated the worst offending stripes, and reduced the noise in the cubes by a factor of approximately 1.1.

Finally, we spatially smoothed the data of UGC 6871 so the final spatial resolution and column density sensitivity was of comparable to those of the other galaxies (see Table 2).

2.3.3 Source finding

In order to create moment maps from the relatively low signal-to-noise data, we used the automated HI source finder SoFiA, the Source Finding Application (Serra et al. 2015). We used the ‘smooth and clip’ method with a large merge radius and pixel dilation to capture the large-scale low surface brightness flux in each galaxy. The source finder works iteratively, to find sources in the data down to a user specified signal-to-noise, mask them, smooth the data, and search again. The mask is iterated upon and grows with each smoothing run. We used kernels which smoothed the data up to only two channels in velocity, since our cubes were already averaged significantly in velocity, and up to 12×12 or 24×24 pixels spatially. This allowed us to identify and include low column density gas in our final images, while the moment maps are presented at full spatial resolution to resolve the central regions of each galaxy.

3 RESULTS

3.1 Optical properties of HIRB galaxies

3.1.1 Bar lengths

The length of a bar is often difficult to define and there is no standard way of measuring it. In this study, we use bar length or refer to twice the bar radius. Commonly used techniques to measure bar sizes are based on (1) visual bar length measurements (used in Galaxy Zoo studies; Hoyle et al. 2011), (2) bar major axis surface brightness profiles (obtained from photometric decompositions; Kruk et al. 2018), and (3) ellipse fits to galaxy isophotes (where the bar length is assumed to be at the maximum of the ellipticity, Sheth et al. 2003; Erwin 2005).

We have used all the three methods to determine the bar sizes for the six galaxies in the HIRB Galaxy Survey. First, we measured the bar lengths using visual estimation directly from the SDSS *i*-band images (which are less prone to dust, and hence better probe the mass distribution). In the second method, the bar size is assumed to

Table 3. Optical properties of the HIRB galaxy sample. Columns: (1) Name of Galaxy, (2) Length of the bar in kpc, (3) Diameter of the disc, (4) Bar to Galaxy ratio, (5) Optical ($u - r$).

Name	Bar length (kpc)	$2r_{\text{Petro}}$ (kpc)	Relative bar length	($u - r$)
(1)	(2)	(3)	(4)	(5)
UGC 4109	14.48	48.26	0.29	2.76
UGC 9362	11.5	30.33	0.36	2.47
UGC 9244	8.22	28.60	0.28	2.75
UGC 6871	6.36	17.55	0.36	2.08
UGC 7383	5.12	14.97	0.30	1.73
UGC 8408	4.26	20.85	0.21	1.81

be the effective radius of a Sérsic fit to the brightness profile along the bar major axis, in a detailed disc + bar + bulge photometric decomposition done in Kruk et al. (2018). The multicomponent decomposition also allows the position angle of the bar and of the disc to be measured. Finally, we used the IRAF ellipse routine to fit elliptical isophotes to the galaxy *i*-band images and determined the bar size at the maximum of the ellipticity. The bar length measurements agree (within ~ 10 per cent of each other). In general, the bar effective radius is shorter than the manually measure bar length, which is shorter than the estimated value based on maximum ellipticity. Henceforth, we use the visually measured bar lengths, which are often the median value of the three measurement methods, while the position angles are based on the disc + bar + bulge decompositions.

While bar length cannot be used as any kind of absolute chronometer for bar age, all simulations show monotonic increase in bar length with time (e.g. Martinez-Valpuesta, Shlosman & Heller 2006; Athanassoula 2013). We order the HIRB galaxies with respect to an increasing absolute bar length (measured in kpc), this is revealed by the colour and numerical coding in all plots (see Figs 1, 3, 4, 6, and 7), we also provide relative bar lengths in Table 3. Neither the absolute nor the relative bar length can be used as a direct proxy for bar age, as there are many other factors that can influence the size of the stellar bar, as well as the speed with which it grows.

3.1.2 Optical morphology

In this section, we provide some discussion and comments on the optical morphology of each of the six HIRB galaxies.

(i) **UGC 8408** is also known as NGC 5115. This HIRB galaxy has the shortest actual bar length at 4.26 kpc, which is less than third of the length of the longest bar in the sample (UGC 4109). While UGC 8408’s bar still covers 21 per cent of the disc’s optical extent, this is the shortest relative bar length of the entire sample, which hints that it might be the most recently formed. UGC 8408 is one of the ‘bluest’ galaxies we observed, it is also the second least massive galaxy with a stellar mass value of $10^{10.2} M_{\odot}$. There is some obvious distortion to the optical morphology of this galaxy. It appears to be a grand design spiral, with two main arms which are clearly defined. However, it seems to also have an extra ‘arm’ which does not quite reach the centre. In the Corwin, Buta & de Vaucouleurs (1994, hereafter RC3), this galaxy was classified as SBcd. This galaxy is shown as the purple ‘1’ icon in all sample plots.

(ii) **UGC 7383** is an obviously blue galaxy. It has a stellar mass of $10^{10.1} M_{\odot}$, making it the least massive of the sample. Accordingly,

UGC 7383 has the second physically shortest bars of the sample at 5.1 kpc, which however still covers 30 per cent of the extent of the optical disc. The optical image of this galaxy shows two defined, tightly wound spiral arms, without much evidence of interaction with any nearby galaxies. The **RC3** classifies this as Sab, which does not account for the bar, spotted by 22 out of 38 GZ2 classifiers. This galaxy is shown as the blue ‘2’ icon in all sample plots.

(iii) **UGC 6871** is central in the range of optical colours and stellar masses of the HIRB sample. It has a stellar mass of $10^{10.6} M_{\odot}$ and appears to be on the blue side of the green valley. Although UGC 6871 is clearly a flocculent spiral, there is a distortion in one of the arms at the lower left of the galaxy. It appears to be stretching out from the galaxy towards the end of the arm. Curiously, the **RC3** classify this as an SB0 (perhaps due to the limitations of photographic images blurring the flocculent arms together), while Nair & Abraham (2010a) classify it as Sc, which does not incorporate the bar. In GZ2, 21 out of 39 classifiers indicated the presence of the bar. The bar is the third shortest of the sample at 6.4 kpc or 36 per cent of the diameter of the disc. This galaxy is shown as the green ‘3’ icon in all sample plots.

(iv) **UGC 9244**: This galaxy has some obvious interaction with a very close neighbour to the north-east. This has resulted in the northernmost spiral arm being significantly distorted. UGC 9244 has two primary arms and a third smaller one. It was classified as SBbc in the **RC3**. It hosts the third longest bar of the sample at 8.2 kpc, or 28 per cent of the diameter of the disc. It has a stellar mass of $10^{10.9} M_{\odot}$, making it the second most massive galaxy of the sample. It is also one of the ‘redder’ galaxies in the sample. This galaxy is shown as the yellow ‘4’ icon in all sample plots.

(v) **UGC 9362**: UGC 9362 is another flocculent spiral galaxy. It was classified as Sbc in the **RC3** on photographic plates, which does not account for the bar (potentially due to resolution issues); 21/28 GZ2 users identified the obvious bar. It has the second longest bar of the HIRB sample, with a length of 11.5 kpc which however covers 36 per cent of the total extent of its optical disc (i.e. more of the galaxy than the bar in UGC 4109). This galaxy, which is the third most massive in the HIRB sample, is optically found in the green valley (close to the red side) and is shown as the orange ‘5’ icon in all sample plots.

(vi) **UGC 4109**, like UGC 6871 and UGC 9244, is a flocculent spiral which was classified as SB(r)b in **RC3**, denoting an Sb type with a strong bar and ring. In GZ2, 41/45 classifiers identified the bar, and four out of five users asked also noted the ring (questions about rings in Galaxy Zoo are in a sub-menu, often missed). According to our measurements, this galaxy has the longest bar of all of the galaxies in the HIRB sample (with a length of 14.5 kpc), which stretches across 29 per cent of the optical extent of the galaxy. This galaxy is also one of the most massive of the sample, with a stellar mass of $10^{11.0} M_{\odot}$, and one of the ‘reddest’ of the HIRBs. This galaxy is shown as the red ‘6’ icon in all sample plots.

3.1.3 Star formation history

The HIRB sample span a range of properties including gas fraction (Fig. 1), galaxy total colour (Fig. 3), and star formation rate (Fig. 4), despite covering a relatively narrow range in stellar mass (approximately one order of magnitude). From Fig. 3, we see that our Galaxies span the blue cloud, green valley, and red sequence. In the following sections, we present the optical properties and HI morphologies in relation to the bar length to attempt to explain how

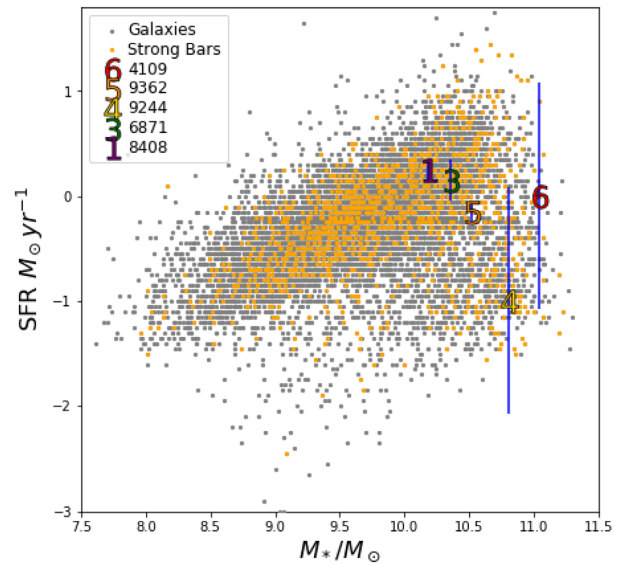


Figure 4. The HIRB galaxies plotted on a star formation rate versus stellar mass (a galaxy star-forming sequence) plot. The grey points show our volume-limited subset of ALFALFA100, while the orange points depict the strongly barred of those galaxies, and the coloured symbols show the HIRB galaxies, with the rainbow and numerical order indicating physical bar length. The error bars indicate the interquartile range.

they vary with the transition of galaxies with a high HI content from the blue cloud to the red sequence.

We explore the star formation properties of the sample further in Fig. 4 which makes use of star formation rates from the MPA-JHU catalogue. These star formation rates are used to plot the ‘star-forming sequence’ of galaxies. We show the entire parent sample (ALFALFA-detected GZ2 galaxies) in grey, with those with strong bars overplotted in orange. Five of the HIRB galaxies are highlighted, the final HIRB galaxy (UGC 7383) has an unreliable flag on its SFR, and so is not plotted, but its optical colours and spectrum suggest it is star forming. We see that only two are clearly on the star-forming sequence, with two just below, and one well off it. This is despite all five having significantly more HI than is expected for their stellar mass.

While the SF rates shown in Fig. 4 have been corrected for H α emission from non- star-forming sources it is reasonable to wonder if the presence of the strong bar might be feeding an AGN in these galaxies through the in-falling gas. This was shown as likely by Oh, Oh & Yi (2012), but disputed by Galloway et al. (2015) and Cheung et al. (2015). According to a diagnostic ‘BPT’ diagram (Baldwin, Phillips & Terlevich 1981), all six of the HIRB galaxies and their companions have line emission which comes almost exclusively from star formation regions. None of these galaxies present any evidence for any emission from an AGN. We also include the plot showing the SFR (as seen in Fig. 4) and the absolute bar length (Fig. 5).

Another useful diagnostic diagram for the optical properties of galaxies is $D_n(4000)$ against $H\delta_A$. This diagram is diagnostic of the fraction of star formation in the last 2 Gyr which occurred in bursts, versus continuous star formation (Kauffmann et al. 2003). $D_n(4000)$ refers to the strength of the 4000 Å break which is a standard indicator of the age of a stellar population, and $H\delta_A$ shows the amount of flux from A stars (associated with star formation about 1 Gyr ago). These values for our data are also found in the MPA-JHU catalogue described for Fig. 4. We show this in Fig. 6,

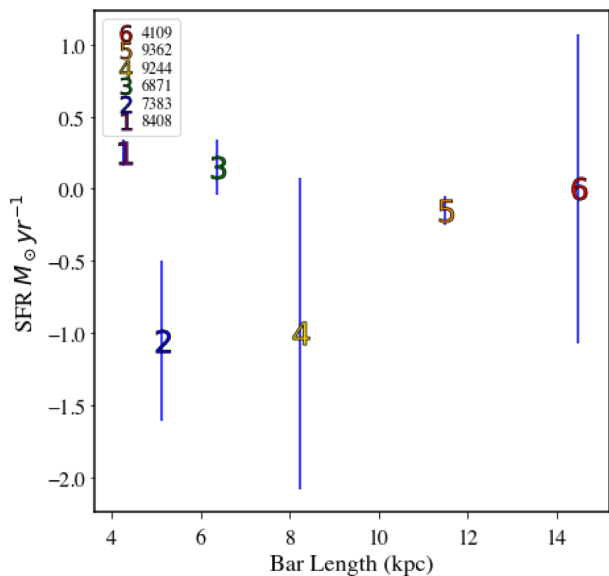


Figure 5. The absolute bar length of each of the six HIRB galaxies against their star formation rates. The error bars indicate the interquartile range.

which compares the position of the HIRB galaxies with similar H I masses (left) or similar bar properties (right). Models from Kauffmann et al. (2003) are indicated, which show regions which are populated by smooth star formation histories (green), currently starbursting (cyan) or post-starburst (blue) galaxies, with emission from galaxies with mixed star formation found in the middle. As is noted, the HIRBs typically lie in the quiescent part of this diagram, as is also normal for galaxies with similar bar properties (at right),

but lie to the low star formation side of galaxies with similar H I masses.

As will be discussed in Section 3.2.2, UGC 4109 (red 6) and UGC 9244 (yellow 4) both have H I holes at their centre. This suggests the bar has already funnelled the gas towards the very centre, which might then lead to a concentration of H₂ in the centre and therefore we expect younger population of stars in the centre (e.g. as was observed by Ellison et al. 2011 in a sample of barred galaxies).

The HIRB galaxies were run through the star formation history software tool STARPY (Smethurst et al. 2015). STARPY employs a Bayesian method along with ensemble Markov Chain Monte Carlo (Foreman-Mackey et al. 2013) to infer the parameters describing a simple exponentially declining star formation history of a single galaxy. STARPY makes use of the SDSS and GALEX optical photometry, specifically the Petrosian magnitude $\text{petroMag } u$ and r wavebands, provided by SDSS Data Release 7 (Stoughton et al. 2002) and the NUV waveband from GALEX (Martin et al. 2005). STARPY requires the observed $u - r$ and $NUV - u$ colours and redshift. Intrinsic dust is not taken into consideration or modelled for. The full description and method can be found in Section 3.2 in Smethurst et al. (2015).

Only five of the HIRB galaxies were able to go through the STARPY software. UGC 6871 was not detected with GALEX; it was right on the edge of a field, meaning that the NUV value was not available. Three of the HIRBs (UGC 4109, UGC 9244, and UGC 9362) have results which suggested they started to quench very early on in their history, and the quenching proceeded slowly so they are probably still star forming. The other two (UGC 8408 and UGC 7383) have begun quenching more recently and relatively rapidly. Fig. 7 shows the HIRB galaxies placement in comparison with the sample used in Smethurst et al. (2015), where we can see that two HIRB galaxies are relatively normal $u - r$ colours, while three are

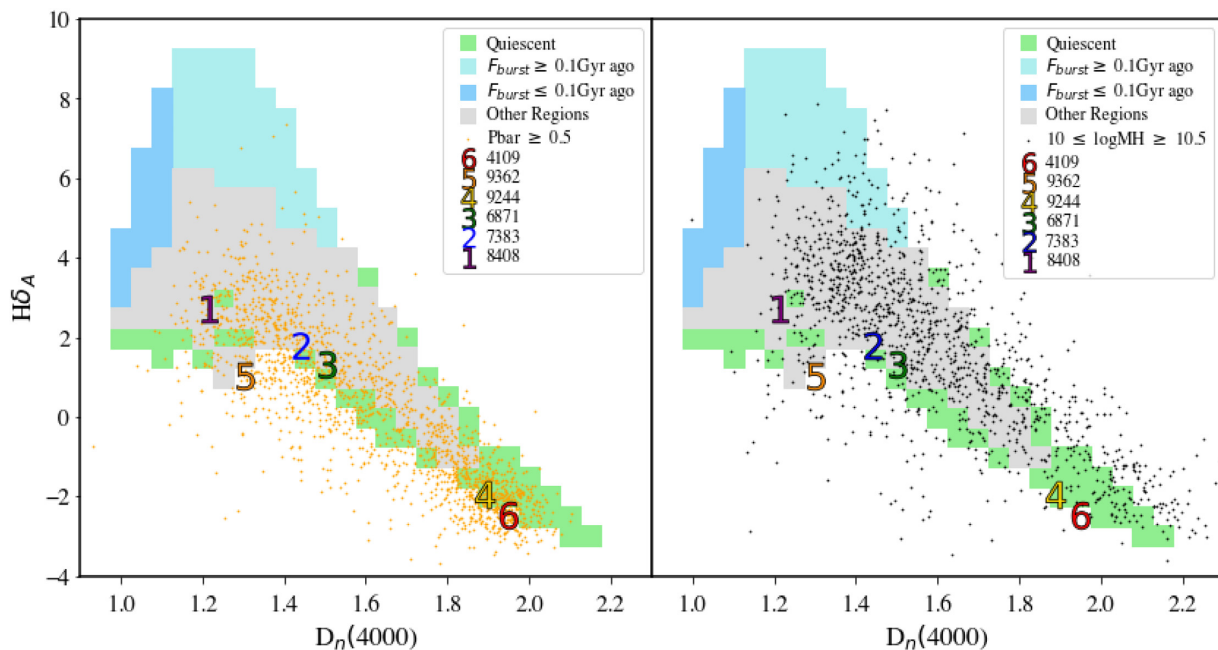


Figure 6. $D_n(4000)$ versus $H\delta_A$ for: Left: all spiral galaxies with a strong bar ($P_{\text{bar}} \geq 0.5$). Right: spiral galaxies with a H I mass range similar to that shown by the HIRB's ($\log(M_{\odot}/M_{\text{H I}}) = 10-10.5$). $D_n(4000)$ correlates with the global stellar population age (larger is older), while $H\delta_A$ peaks in post-starburst galaxies. The background colours show models of Kauffmann et al. (2003); green for quiescent galaxies, cyan for starburst galaxies (burst occurred less than 1 Gyr ago), blue shows post-starburst galaxies (burst occurred over 1 Gyr ago), and grey are all other regions covered by the model galaxies Kauffmann et al. (2003). These values are from the 3 arcsec SDSS fibre, so we probe the stellar population in the bulge. As with the other figures, the individual HIRB galaxies are shown by different numbers and colours.

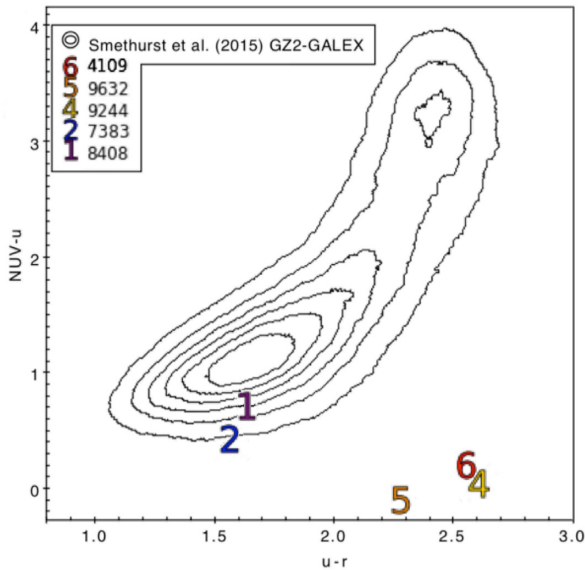


Figure 7. A $NUV - U$ versus $u - r$ plot for the five galaxies that were run through STARPY. Compared to the Smethurst et al. (2015) sample, three HIRB galaxies (UGC 4109, UGC 9362, and UGC 9244) are very optically red in comparison to their blue NUV colours.

very red in $u - r$ for their $NUV - u$ colours indicating the extremely slow quenching.

While the star formation properties and stellar ages revealed by the optical data on HIRB galaxies do not show a monotonic increase with bar length, there is clearly a general trend such that those HIRB galaxies with longer bars (red, orange, and yellow) are more likely to be passive and have old stellar populations for their stellar mass than those with shorter bars (blue and purple). This is particularly evident in Fig. 7 where the two groups show quite different quenching histories.

3.2 H I properties of HIRB galaxies

3.2.1 H I masses from synthesis imaging

We measure the H I mass for each galaxy in the HIRB sample using the interferometers (VLA and GMRT), and ALFALFA had already measured the H I mass using the single dish telescope, Arecibo. The masses we measured differ by small amounts to the masses from ALFALFA, but this may be unsurprising given the differences in observing techniques. ALFALFA's M_{HI} is shown in Table 1, column 6, and the M_{HI} measured from the resolved H I data can be seen in Table 4, column 3. ALFALFA's measurement was larger in four of the cases (UGC 9362, UGC 9244, UGC 6871, UGC 8408). In the other two, where ALFALFA's H I measurement was lower than that collected by the interferometer (UGC 4109 & UGC 7383), the data were collected both times by the VLA rather than the GMRT. A comparison between the H I masses measured between the single dish and the interferometer can be seen in Table 5. The H I mass and errors from the single dish data were obtained from the ALFALFA survey (Haynes et al. 2011) and the H I masses and errors from the data described in this paper. We estimate a roughly 20–30 per cent error on the interferometric fluxes due to a number of factors, including the continuum subtraction, small residual calibration errors, missing flux due to the lack of short baselines (specifically UGC 6871,

where a 50 per cent uncertainty is estimated), and limitations in sensitivity.

In all cases, we believe the ALFALFA mass is more likely to be a good measurement of the total H I mass. Single dish radio observations will collect and measure all of the H I detected within the beam, which is significantly larger than the beam of interferometers like the VLA and the GMRT. This means the measured M_{HI} value may include some of the flux from H I in other nearby galaxies or structures and are too nearby to differentiate between. While reducing resolved H I data, we can disregard some of the H I we can see is coming from other structures, however synthesis imaging will also resolve out some of the low surface brightness signal received. Because of this, synthesis imaging is known to miss H I mass, and it is common practice for the single dish data to be treated as more reliable measure of total H I mass. We have determined that the nearby galaxies to the HIRB galaxies are outside the Arecibo beam. You could add something along the lines of typical uncertainties on H I mass are about 10–15 per cent (Springob et al. 2005), and we expect our uncertainties are closer to 20 per cent due to the low signal to noise of the diffuse gas in the outskirts of the galaxies, on top of the fraction of gas we are missing due to the relative lack of short baselines.

3.2.2 H I morphology and velocity field

In this section, we will describe the H I morphology and content from our VLA/GMRT observations. According to simulations (Athanasoula 2013), there exists a correlation between gas fraction, the rate of development of a strong bar, the bar's formation time, and the morphology of the H I remaining in the galaxy. Specifically, the higher the gas fraction, the longer it takes for a bar to develop thus the central H I hole also develops at a later stage in the galaxy's life. This means that we should be more likely to see these H I holes in the galaxies with the lowest gas fractions. In this section, we investigate if this correlation is also present from the data collected by the HIRBs survey.

The H I gas fractions ($M_{\text{HI}}/(M_{\text{HI}} + M_*)$) for our six galaxies are shown in Fig. 3, and the morphologies shown for each HIRB galaxy in Figs 8 and 9. We also summarize these data in Table 4.

It is clear from Figs 8 and 9 that there is a variety of H I morphology revealed by the HIRB galaxies. Fig. 10 shows the intensity of H I in a slice aligned at the position angle of the bar; the highlighted region shows exactly where the bar is to aid in our description of how H I morphology relates to the position of the bar.

Both UGC 9362 and UGC 9244 show clear large scale holes in their centres and Fig. 10 shows the absence of any significant amounts of H I in their bar regions at all.

While UGC 4109 and UGC 6871 show large-scale H I holes, they appear to be significantly offset from their centres. However, when looking at the highlighted region in Fig. 10, we can see that there is still a dip in both of these galaxies' H I intensity at the position of the bar. This could suggest that the bar is working towards sweeping the central region, but this still does not offer an explanation for the source of the large offset hole. It may be that tidal disruption plays a role in the H I morphology shown in these two galaxies.

UGC 4109 has also been observed by the VLA in C-configuration in Lemonias et al. (2014). Named GASS 51390 in that study, they show the H I intensity map in their fig. 6. While this C configuration has lower spatial resolution than our data, we can clearly see there exists a hole in H I. Our observations reveal that the hole is slightly

Table 4. Our measurements of H I properties of HIRB Galaxies using the GMRT/VLA. Columns: (1) Name of Galaxy (2) Central velocity of H I detection, (3) H I mass, (4) Number of companion galaxies found in the resolved H I data, (5) Whether or not a hole in the H I is present.

Name	Central $v_{\text{H I}}$	$\log M_{\text{H I}}/M_{\odot}$	# of H I companions	H I Hole Detected?
(1)	(2)	(3)	(4)	(5)
UGC 4109	13087	10.62	0	Offset hole
UGC 9362	8528	10.00	1	hole
UGC 9244	8106	10.11	1	hole
UGC 6871	6460	10.03	0	Offset hole
UGC 7383	7177	10.59	2	No hole
UGC 8408	7093	10.07	0	No hole

Table 5. Our measurements of $\log(M_{\text{H I}}/M_{\odot})$ of HIRB Galaxies using the GMRT/VLA compared to the $\log(M_{\text{H I}}/M_{\odot})$ measurements taken by ALFALFA. Columns: (1) Name of Galaxy (2) $\log(M_{\text{H I}}/M_{\odot})$ from ALFALFA, (3) The error of ALFALFA’s measurements, (4) $\log(M_{\text{H I}}/M_{\odot})$ from the GMRT/VLA, (5) The error on our measurements.

Name	Single Dish $\log(M_{\text{H I}}/M_{\odot})$	Error	Interferometer $\log(M_{\text{H I}}/M_{\odot})$	Error
(1)	(2)	(3)	(4)	(5)
UGC 4109	10.46	± 0.05	10.62	± 0.11
UGC 9362	10.34	± 0.05	10.00	± 0.11
UGC 9244	10.36	± 0.05	10.11	± 0.11
UGC 6871	10.29	± 0.05	10.03	± 0.24
UGC 7383	10.38	± 0.05	10.59	± 0.11
UGC 8408	10.26	± 0.05	10.07	± 0.11

offset from the centre. On the opposite side to the offset hole there is a denser region – it is possible that a minor merger has occurred resulting in the unusual H I morphology.

UGC 7383 and UGC 8408 are the HIRB galaxies with the two lowest bar lengths, and neither appear to have a hole in the centre of their H I. Looking at the intensity along the exact section of the bar, there is still no evidence of any significant dip in the H I intensity. UGC 8408 on the other hand does have a dip, albeit small enough to not notice when looking solely at the intensity map. So perhaps the bar is working to clear the middle of gas after all.

Our VLA observations of UGC 6871 did not detect all the gas associated with the blue-shifted side of the galaxy. This is evident from the H I spectrum in Fig. 9 (top row, fourth column), in which the emission which is blue shifted with respect to the systemic velocity of the galaxy is seen in the ALFALFA spectrum, but missing from the VLA spectrum. Examining the H I intensity map overlaid on the optical image (Fig. 9), we see that the blue-shifted side of the H I disc (north-west) is not as extended compared to the stellar disc, as the red-shifted side of the gas disc is. Initially, we thought this asymmetry was tidal in origin, however, given the missing flux in the H I profile, we suspect that the gas may be present, but at a column density below what we detect in the VLA observations.

In the first panel for each galaxy (Figs 8 and 9), we overlay a conservative threshold for the H I density typically associated with star formation ($10 M_{\odot} \text{pc}^{-2}$, shown by the black contour; Schaye 2004). In UGC 4109, the majority of this higher density H I is found to the left of the hole in the H I, in a dense region. UGC 9244 and UGC 6871 reach the star formation threshold in many places in the H I however their bar region H I holes are quite evident. Our two blue galaxies with the shortest bars, UGC 7383 and UGC 8408, have H I

above the star formation threshold throughout their discs, which fits with the picture of them forming stars throughout. Finally, UGC 9362 is the only one of the six HIRB galaxies which does not reach this star forming in any significant area (there is a small part which does around RA: $14^{\text{h}}33^{\text{m}}18.5^{\text{s}}$, Dec.: $3^{\circ}54'$ but it is too small to be of any significance morphologically). This galaxy does however appear to be forming stars, which must be happening at a lower H I surface density than is typical.

H I observations also provide velocity fields. We can see that the velocity field for four of the HIRB galaxies are rotating regularly (UGC 4109, UGC 9244, UGC 7383, and UGC 8408). The remaining two galaxy’s velocities (UGC 9362 and UGC 6871) appear to be somewhat distorted. In UGC 9362, the ‘bluer’ velocities are distributed through the middle velocities (green) rather than collected on one side. Similarly, UGC 6871’s ‘redder’ velocities are concentrated in the middle of the galaxy rather than being on one side showing rotation. There is a clear disruption in the gas’s regular rotation. It is possibly that the source of this distortion is nearby companions to these galaxies; this will be explored in a future paper (Newnham et al., in preparation).

3.3 Resolution

Simulations show that bars create H I holes by driving gas flows into the centre of the galaxy. Looking specifically at Athanassoula et al. (2013; fig. 4), they show that the diameter of the hole in the H I is roughly equal to the length of the bar, or slightly smaller. When drawing conclusions from resolved H I data like we have for the HIRB galaxies, it is important to ensure that our resolution is good enough to resolve the H I hole if it exists, as well as other structures present. In this section, we completed a series of resolution tests to check the robustness of our findings from the previous section.

As we can see from Column 4 in Table 6, each HIRB galaxy has a different physical resolution with respect to the length of the bar. Two galaxies do not appear to have a hole in their H I (UGC 7383 and UGC 8408); we need to find out if they truly do not have a hole of a comparable size to the other galaxies, or a hole could be present but not visible due to the resolution. We smoothed our data which had a higher resolution with respect to the size of their bars, to the same bar length/resolution ratio as the worst resolved galaxy in our sample.

We use the data for three of the galaxies which show the prominent holes in the H I: UGC 4109, UGC 9362, and UGC 9244. UGC 7383 has the lowest bar length/resolution value at

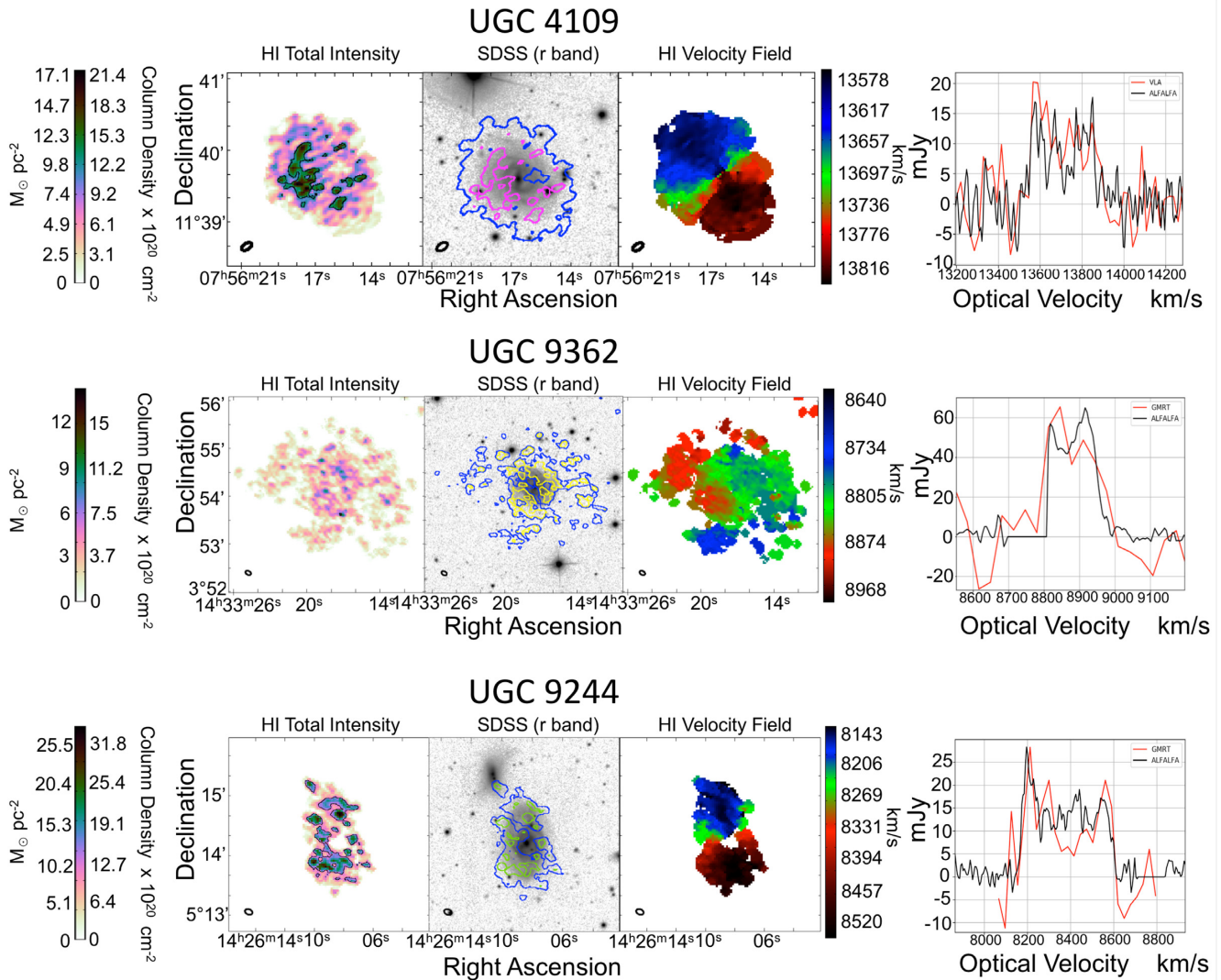


Figure 8. HI resolved data visualized for UGC 4109, UGC 9362, and UGC 9244. For each galaxy the panels from left to right are: (1) The HI total intensity map depicting the column density of each pixel. The black contour depicts the star formation threshold at $10 M_{\odot} \text{pc}^{-2}$ (Schaye 2004), (2) The SDSS *r*-band optical image of the galaxy in grey-scale with the contours of the HI total intensity map overlaid. Contour colours are: blue = 3σ , yellow = 5σ , green = 8σ , magenta = 10σ , cyan = 20σ , orange = 30σ , red = 50σ . (3) The HI velocity field of the galaxy, expressed in km s^{-1} . (4) A comparison of the HI ‘double peak’ detected originally by ALFALFA (black) and by our observation with the VLA/GMRT (red).

0.88 (Table 6, Column 4), meaning that the presence of a hole the size of the bar could potentially be unresolved. We make the maps for UGC 4109, UGC 9361, and UGC 9244 have the same bar length to resolution, respectively, and inspect whether or not the holes are still evident. We reduced the resolution of UGC 4019 by $1.9\times$ ($16.9 \text{arcsec} \times 9.7 \text{arcsec}$), UGC 9362 with $2.8\times$ less resolution ($20.7 \text{arcsec} \times 13.6 \text{arcsec}$), and UGC 9244 with $2.3\times$ ($17.9 \text{arcsec} \times 12.2 \text{arcsec}$).

The holes in the HI of these three galaxies can still clearly be seen in UGC 4109 and UGC 9244. The hole is less clear in UGC 9362 but there is still a very noticeable dip in density in the central region. Based on this, we can be confident that there are no holes currently in the centres of UGC 7383 and UGC 8408 to the depth and size of the holes in these three galaxies, as there are no noticeable dips in the column density (Fig. 10). As mentioned above, UGC 7383 in Fig. 10 does show a small dip in the column

density; based on these results, this dip may be deeper than what our low-resolution observations suggest, but it is unlikely to be a full hole yet.

We also looked at the data for a more nearby galaxy, outside of the HIRB sample, to see if reducing the resolution could hide the hole. M95 has been observed with the VLA as part of the THINGS survey⁶ (Walter et al. 2008). Of this survey, it is the only galaxy to have a strong bar, a large HI mass, and a prominent central hole. Despite all the features that are no longer visible in the lower resolution image, the central HI hole is still extremely clear.

⁶All the data for the THINGS galaxies are publicly available at <http://www.mpia.de/THINGS/Data.html>.

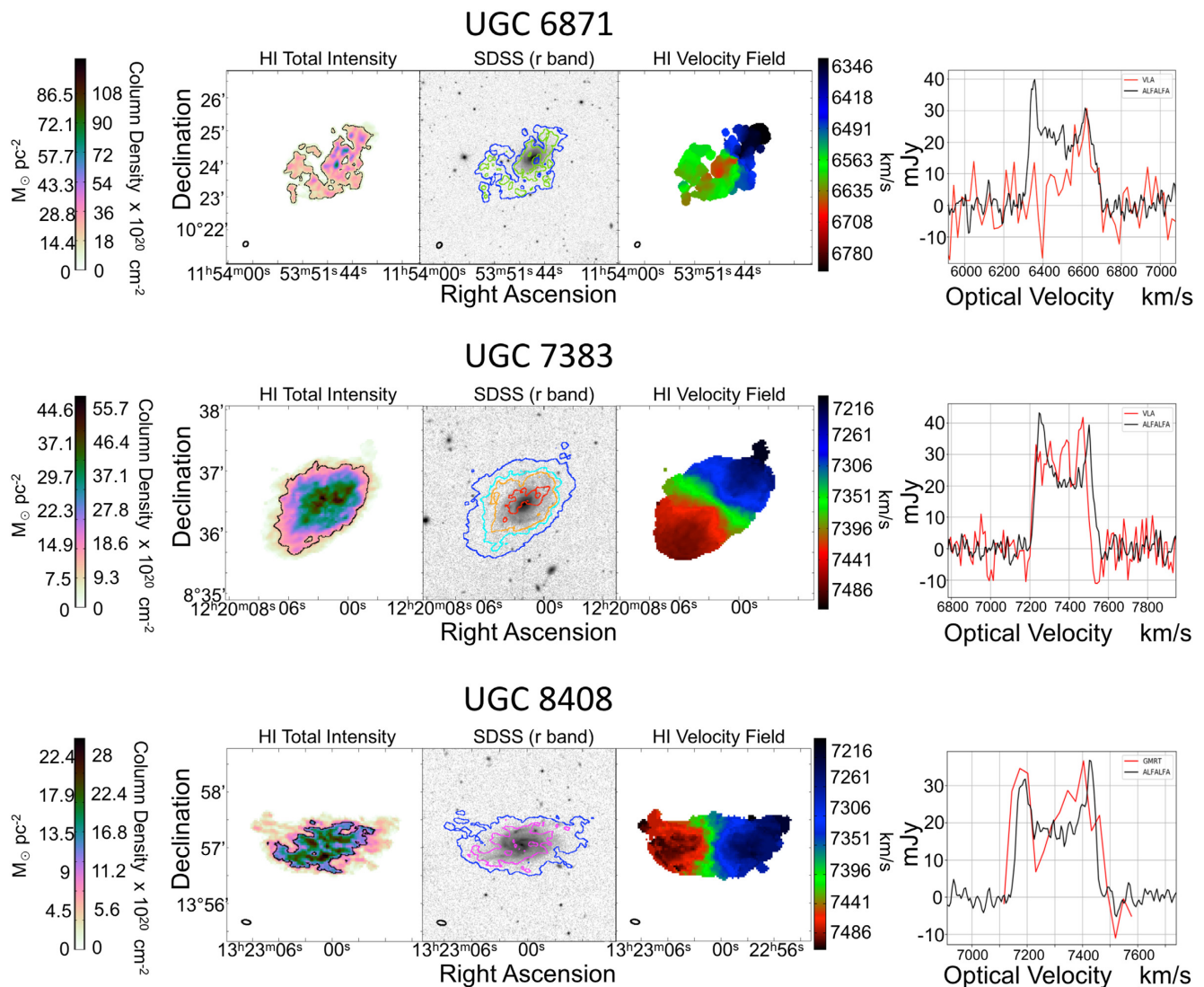


Figure 9. H I resolved data visualized for UGC 6871, UGC 7383, and UGC 8408. For each galaxy the panels from left to right are: (1) The H I total intensity map depicting the column density of each pixel. The black contour depicts the star formation threshold at $10 M_{\odot} \text{ pc}^{-2}$ (Schaye 2004), (2) The SDSS *r*-band optical image of the galaxy in grey-scale with the contours of the H I total intensity map overlaid. Contour colours are: blue = 3σ , yellow = 5σ , green = 8σ , magenta = 10σ , cyan = 20σ , orange = 30σ , red = 50σ . (3) The H I velocity field of the galaxy, expressed in km s^{-1} . (4) A comparison of the H I 'double peak' detected originally by ALFALFA (black) and by our observation with the VLA/GMRT (red).

4 DISCUSSION

The HIRB study was initiated with the goal of investigating what a strong bar does to a gas-rich galaxy, or equivalently what a significant quantity of gas in a galaxy does to the evolution of a strong bar.

Bar quenching is an idea which has been around in the literature for some time (e.g. Tubbs 1982) but has recently gained more attention due to the observation that passive spirals have large bar fractions (Masters et al. 2010), the strong trend of bar fraction with optical colour (Nair & Abraham 2010a; Masters et al. 2011), and suggestions that bars can drive secular growth of bulges, a morphological characteristic long agreed to correlate with quenched star formation (e.g. Cheung et al. 2013; Kruk et al. 2018). Simulations of the impact of a bar on gas in a galaxy demonstrate its ability to redistribute gas (e.g. Berentzen et al. 1998; Combes 2008;

Villa-Vargas et al. 2010; Athanassoula et al. 2013), more recently simulations have explicitly explored the possibility for these flows to lead to global SF quenching (Gavazzi et al. 2015; James & Percival 2016; Spinoso et al. 2017; James & Percival 2018; Khoperskov et al. 2018). However, there is also a possibility that the torques from the bar simply prevent gas from collapsing and forming stars at the typical thresholds for star formation (e.g. the model initially proposed by Tubbs 1982).

In Athanassoula (2013), a galaxy's gas fraction was found to be influential in the rate of development of the bar itself, with higher gas fractions delaying the formation of the bar, and resulting in weaker bar. Evidence of this link between gas fraction and the suppression of bar formation is present in observations which show that bars are less likely to be found in gas-rich spirals (or equivalently that barred galaxies have lower gas content; Masters et al. 2012; Kim et al. 2017).

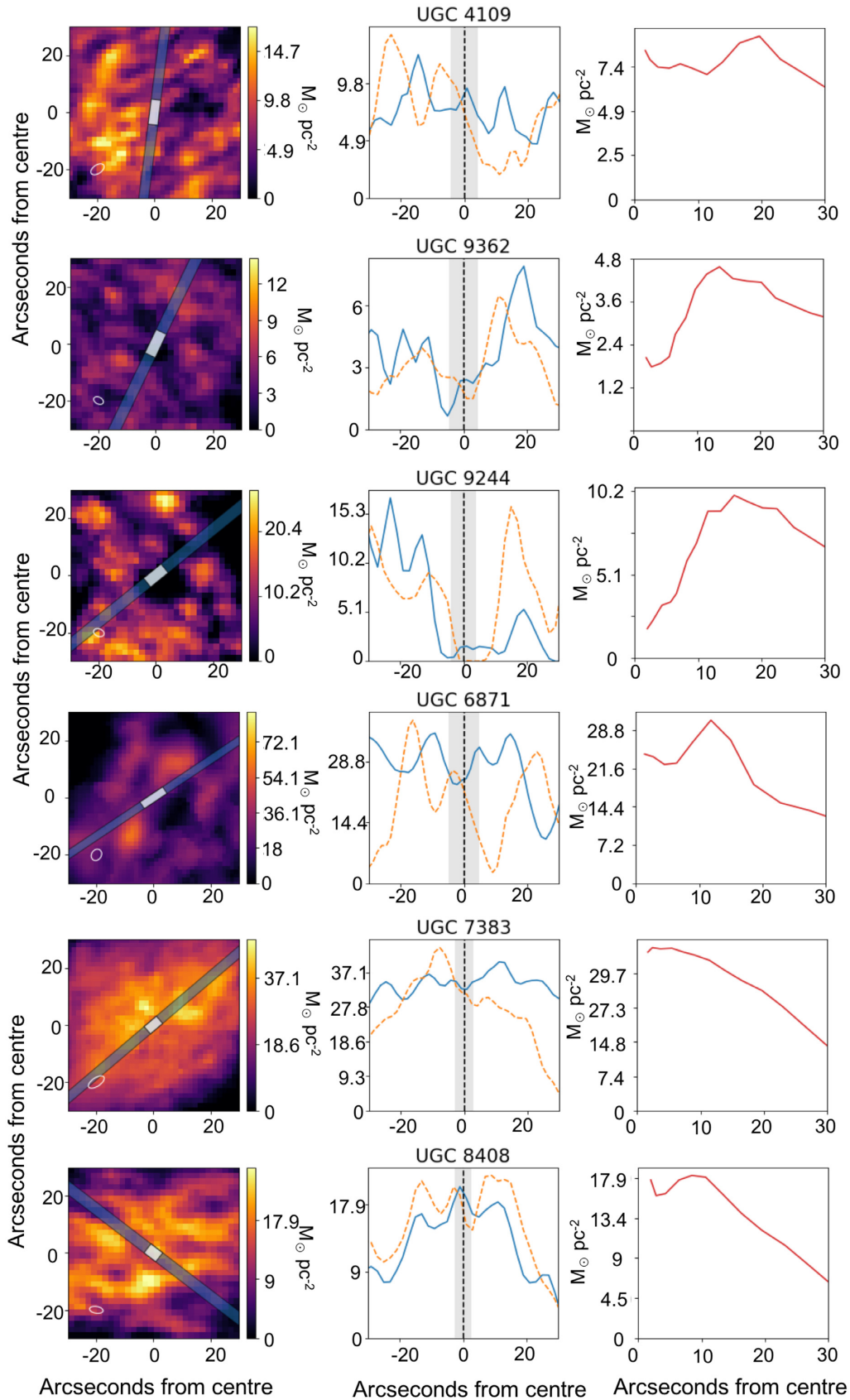


Figure 10. Left: The H I density map of each galaxy. Middle: A slice from the data is then taken along the bar (blue) and perpendicular to the bar (orange dashed) and the H I density is then plotted. The area of the bar is highlighted. Right: the azimuthal average.

Table 6. Resolution properties of the six HIRB galaxies. Columns: (1) HIRB Galaxy name, (2) Resolution of image in arcsec, (3) Bar length in arcsec, (4) Bar length/Resolution, (5) Bar length in kpc, (6) Physical resolution in kpc, (7) Presence of a hole in the H I.

Name	Resolution arcsec	Bar length arcsec	Bar/res	Bar length kpc	Physical resolution kpc	H I hole Detected?
(1)	(2)	(3)	(4)	(5)	(6)	(7)
UGC 4109	8.9×5.1	15	1.7	14.4	8.6×4.9	Hole
UGC 9362	7.3×4.8	18.2	2.5	11.5	4.6×3.0	Hole
UGC 9244	7.8×5.3	15.8	2.02	8.2	4.0×2.8	Hole
UGC 6871	10.1×8.2	13.4	1.3	6.4	4.8×3.9	Hole
UGC 7383	10.9×5.1	9.6	0.88	5.1	5.8×2.8	No hole
UGC 8408	9.6×4.8	10.4	1.08	4.3	3.9×1.9	No hole

We seek to use observations of H I morphology to provide constraints on the mechanism of bar quenching, and to understand how unusual galaxies with high gas fractions and strong bars came to be. If gas redistribution is the main mechanism we might expect to see clear evidence for it in the H I morphology (e.g. central holes), while if H I gas is present in large quantities and above the typical threshold for star formation ($\sim 3\text{--}10 M_{\odot} \text{pc}^{-2}$, Schaye 2004) in galaxies where star formation is suppressed, we can argue that bar torques preventing the gas from cool may be more important.

Gas-rich and strongly barred galaxies have not been specifically studied with resolved H I observations; since these galaxies are rare, they are unlikely to come up in a sample selection unless specifically put in it. Studies that look at gas-rich galaxies tend not to consider morphology, leading to these rare galaxies being missed, then studies with a morphology focus often include strongly barred galaxies but those are rarely gas-rich unless intended to be so. However, there are some resolved H I observations of very nearby galaxies with strong bars.

The H I Nearby Galaxy Survey (THINGS) (Walter et al. 2008) survey reaches typical column densities of $4 \times 10^{19} \text{cm}^{-2}$, which is comparable to the column densities we reach with the HIRB sample. They present observations for one of HIRB-like strongly barred galaxy, M95, showing in extreme detail the distribution of the H I throughout the galaxy revealing a H I hole (and a small H I concentration in the very centre was also found). Recently, George et al. (2018) took these data, along with other multiwavelength data for M95 to argue that redistribution of gas is likely to be the main process for bar quenching in M95 (rather than heating from bar torques).

The proto-typical strongly barred galaxy, NGC 1300, also has resolved H I data, taken in the 1980s with the VLA (England 1989). A re-analysis of those data show clearly the H I hole and gas streaming (Lindblad et al. 1997). A large H I hole is also observed in nearby barred galaxies NGC 3992 (Bottema & Verheijen 2002) and NGC 7479 (Laine & Gottesman 1998), and while there is clear hints of a H I hole in the data on NGC 4123 presented by Weiner, Sellwood & Williams (2001) they also note evidence for shocks caused by gas flow in the bar region. Contrary to this, the H I morphology in the very-late-type barred spiral, NGC 3319, does not show a central hole, but rather gas and star formation all along its bar (Moore & Gottesman 1998). This difference is explained by Moore & Gottesman (1998), NGC 3319 being a dynamically younger galaxy than the early-type spirals with strong bars, obvious H I holes, and lower gas fractions. Indeed, it has a significantly higher gas fraction than the other galaxies (56 per cent compared to 6 per cent gas in M95). It is worth noting that all of these very

nearby galaxies with resolved H I have typical (or even low) H I gas fractions for their stellar mass, unlike our HIRB sample which are all at least 3σ gas-rich outliers in the H I mass to stellar mass relation [see Fig. 1, where all HIRB galaxies are well above the mean line, while these galaxies (not shown) would be on or below it].

We will now discuss how the data presented in this paper for HIRB galaxies support, or reject the plausible bar quenching mechanisms of gas redistribution and/or heating due to bar torques in very-gas-rich galaxies.

We particularly compare our observations to the simulations of Athanassoula (2013). In that work, it is shown that the time taken to develop a H I hole will vary from galaxy to galaxy, and also depends on the details of the gas fraction in the galaxy, with observable H I holes being slow to develop in gas-rich galaxies even in the presence of a strong bar. In that work, the most gas-rich galaxies did not develop clear H I holes by the end of the simulation (at 10 Gyr). It is also known that the bar mass impacts the ability of a bar to evacuate H I, with Hunter (1990) showing that a bar needs to hold about 10 per cent of the disc mass to make a central H I depression.

We start by now considering the sample in order of H I gas fraction and compare to the gas morphology and time-scales shown in fig. 4 of Athanassoula (2013):

(i) **Gas fraction ~ 20 per cent:** From the simulations of Athanassoula (2013), all strongly barred galaxies that have a total gas fraction around 20 per cent develop the hole in the centre of the H I by 6 Gyr after the formation of a strong bar. The HIRB sample's two most gas-poor galaxies UGC 4109 and UGC 9244 with H I gas fractions of 21 per cent and 17 per cent show an offset hole, and central hole, respectively (Figs 3 and 8). These galaxies are therefore consistent with being at this stage of their evolution where they formed a bar at least 6 Gyr ago. These are also our two globally reddest galaxies, suggesting a global cessation of star formation; this is backed up, for the central bulge region at least, by their fibre spectra which reveal old central stellar populations (Fig. 6), and further while UGC 4109 (with an offset hole) is only just below the star-forming sequence; UGC 9244 which has the largest central H I hole is well below the star-forming sequence (see Fig. 4). M95, with a gas fraction of 6 per cent by mass (Leroy et al. 2008), appears to be another example of this type of dynamical advanced galaxy with a strong bar.

(ii) **Gas fraction $\sim 35\text{--}45$ per cent:**

Three of our Galaxies have H I gas fractions around 35–45 per cent. One of these galaxies is in the redder edge of the green valley, one in the bluer edge, and one in the blue sequence, as seen in Fig. 3, with UGC 9362 (orange ‘5’) on the red side, UGC 6871 (green ‘3’) on the blue side, and UGC 8408 (purple ‘1’) well in the blue cloud.

According to the simulations of Athanassoula et al. (2013), a galaxy with 50 per cent of its disc mass in cold gas and a bar which formed at least 6 Gyr ago would already have a noticeable hole in the centre. Indeed, both UGC 9362 (orange ‘5’) and UGC 6871 (green ‘3’) have central H I holes (although UGC 6871’s is offset from the centre), however UGC 8408 (purple ‘1’) does not. This suggests the bar in UGC 8408 may be dynamically younger than those in both UGC 9362 and UGC 6871, and UGC 8408’s more vigorous star formation and younger stellar population paints a similar picture of a dynamically younger galaxy.

(iii) **Gas fraction ~ 70 per cent:**

Our most gas-rich galaxy, UGC 7383, despite having a stellar mass of $M_* \sim 10^{10} M_\odot$, where gas fractions of around 30–40 per cent are more typical, has a gas fraction of 66 per cent (Fig. 3) and displays no evidence for a H I hole in the centre. However, looking at the most gas-rich galaxies simulated in Athanassoula et al. (2013), we would not expect to see a H I hole in this type of galaxy unless the bar formed more than 10 Gyr ago, as galaxies with these high gas fractions were not observed to form a H I hole before the end of the simulation.

Overall, our observations support a picture where bar formation is delayed, and therefore the development of a corresponding H I hole is delayed in galaxies with very high gas fractions, but that bars are apparently acting to clear H I holes in the centres of galaxies and therefore accelerate the cessation of star formation globally.

We will now look at how the star formation properties and optical morphology of the galaxies correlate with the H I morphology. If the development of H I holes are driving bar quenching in HIRB galaxies we would expect that those with holes are under star forming relative to typical galaxies with their properties, while those without holes may be more normal.

In fact, most of the galaxies in the HIRB sample appear to be relatively quiescent, with only two of them appearing in the middle of the star-forming sequence (Fig. 4), despite their large H I reserves. They also show a range of global optical colours.

(i) **Dynamically old bars (H I hole):**

Two of the HIRBs show obvious central H I holes (UGC 9362, orange ‘5’ and UGC 9244, yellow ‘4’; Fig. 10), while two have apparently offset H I holes (UGC 4109, red ‘6’ and UGC 6871, green ‘3’). These four have the longest physical bars (both absolute and relative to their disc size) again supporting a picture that their bars are dynamically the oldest among the HIRB galaxies.

They do however show a range of star formation properties, with UGC 9244 (yellow ‘4’) well off the star formation sequence, UGC 9362 (orange ‘5’) and UGC 4109 (red ‘6’) at the lower edge, and UGC 6871 (green ‘3’) appearing to still be forming stars at a typical rate. Looking at D_n4000 as a tracer of stellar population age we again see two galaxies with clearly old populations (UGC 4109, red ‘6’ and UGC 9244, yellow ‘4’), while the other two are younger. Finally, the analysis of likely quenching history using the technique of Smethurst et al. (2015) reveals that the three galaxies with H I holes where this could be done (UGC 6871 did not have a *GALEX* observation) show a clear signature of unusually slow quenching (red $u - r$ colours, while remaining relatively blue in $NUV - u$; see fig. 7).

All in all this supports the idea that a H I hole correlates with secular (slow) quenching of star formation, possibly caused by bar driving gas clearing, however the details of the individual galaxies are perhaps not surprisingly hinting at a more complex picture.

We will come back to the role of local environment in more detail in a future paper (Newnham et al., in preparation), but it is clear

from the H I morphology and detections of companions in the wider field of our data that local interactions may play a role in the history of these galaxies. For example, looking at the H I distribution in UGC 9244 (Fig. 8, bottom row, first panel), we can see that it is clearly interacting with a lower mass companion. The H I gas is extended in the direction of the companion, distorting the gas from an elliptical shape. This corresponds with the distortion of the spiral arm, visible in the optical image of this galaxy (Fig. 2, lower right). There is also evidence of interaction in the H I morphology of UGC 9362 with its nearby companions, NSA 18045 (Fig. 8, middle row, first panel). Although the data have not picked up any evidence of a H I bridge between the two, we can see that the H I in NSA 18045 is heavily concentrated in the side of the galaxy closest to UGC 9362.

We have not commented on a mechanism which might create an offset H I hole not centred on the bar, or galaxy (as seen in both UGC 4109 and UGC 6871). This may again point to some tidal distortions caused by interactions, and perhaps gas-rich low-mass companions are the reasons for HIRBs having such high gas fractions relative to their other properties. Curiously though, UGC 4109 has no companions which appear local enough to this galaxy to account for its distortion, and its H I velocity field is very regular, so that explanation seems unlikely in this case. The other HIRB galaxy with an offset H I hole, UGC 6871, is also fairly isolated and while its H I velocity field looks quite disturbed, we think the VLA data may have missed some lower column density H I on the blue-shifted side which was detected in the single dish data.

(ii) **Dynamically young bar (No H I hole):**

Both of our HIRB galaxies with no evidence for H I holes (UGC 7383; blue ‘2’, and UGC 8408; purple ‘1’) also have shorter physical bars (and the highest gas fractions) supporting a picture where the gas has delayed bar formation, and the bar has not yet had time (or perhaps is not massive enough) to sweep out cold gas in the bar region.

These galaxies are both optically blue, and UGC 8408 is found on the normal star-forming sequence (UGC 7383 has an unreliable flag in the MPA-JHU derived star formation so we cannot comment on its relative location on that diagram), they also both have relatively young population ages, and in the models of Smethurst et al. (2015) appear on the main locus of points with evidence perhaps for recent quenching. The bar which has not swept out a H I hole in either of these, perhaps does not create enough heating to prevent star formation in them either.

It is possible that the H I holes observed in this work are fully or partly filled with molecular gas. The observations on the HIRB galaxies thus far have not included CO observations, thus cannot detect the presence of molecular gas in the central region, if there is any. Bigiel et al. (2008) study the holes in the H I of the THINGS (Walter et al. 2008) galaxies, and find many of them to contain some molecular gas. However, these holes typically were along the spiral arms of the galaxy, and in other areas of the disc rather than central holes. M95, as discussed earlier, is another example of a H I-rich and barred galaxy which displays a central hole in its H I morphology profile, within which, a small concentration of molecular gas was detected. There has also been a strong correlation between galaxy colour and the amount of CO in galaxies (Saintonge et al. 2011). The reddest of the HIRB galaxies, also have a large hole in the centre, but due to the relation found by Saintonge et al. (2011), there is a slimmer likelihood of the central holes being filled with molecular gas. Future work into this sample hopes to involve CO observations, which will provide the morphology of the molecular gas in these galaxies.

Despite their higher than average H I content (at least 3σ above the average H I content for their stellar mass as shown in Fig. 1), not all of the HIRB galaxies are actively star forming. Our observations of the H I morphology of HIRB galaxies support a picture where as a bar forms, grows, and develops it sweeps out a hole in the H I gas. The central gas will be displaced quicker the lower the gas fraction of the galaxy, i.e. UGC 4109 and UGC 9244 both have a low gas fraction and have evidence of a hole at their centre (UGC9244) or offset slightly (UGC 4109). So for those two galaxies the bar did not necessarily have to age significantly before the H I morphology had been disrupted. This also fits with our two galaxies with the shortest bars, neither UGC 7383 nor UGC 8408 have obvious holes in the centre and happen to be the galaxies with the highest gas fractions in the sample. This suggests that bars need more time to grow to be able to sweep out the gas from the centre. We can see a slight indent in the intensity of the H I in the centre of these two galaxies (Fig. 10) which might hint that the bar is starting to clear the gas. As seen by their range of optical colours (Fig. 3) and the inconsistencies with the star formation trends (Fig. 4), these galaxies are in the transition from being star forming and blue, becoming red and ceasing to form stars due to the presence of the bar.

5 CONCLUSIONS

We have collected, reduced, and imaged resolved H I data for six galaxies making up the HIRB galaxy survey. The galaxies were selected using the ALFALFA survey and GZ2 morphologies, using the parent sample defined in Masters et al. (2012), and found to have a H I mass in the range $10.25 < \log(M_{\text{H I}}/M_{\odot}) < 10.47$. These values correspond to extremely high gas fractions for galaxies of these stellar masses, with the gas fraction ($M_{\text{H I}}/M_{*}$) more than 3σ above the average for their M_{*} . Strongly barred galaxies were selected using the GZ2 bar ‘probability’ of $p_{\text{bar}} > 0.5$ which selects strong bars. Due to the time constraints of observations and data reduction, we selected the nearest 10 of these galaxies, and for six of them we were able to obtain H I total intensity and velocity fields for using with the GMRT or the VLA. These six galaxies have a range of optical colours and bulge sizes, making the sample representative of the local massive spiral population.

The HIRB galaxies show a variety of star formation properties, despite the presence of a strong bar, which usually correlates with passive spirals (Masters et al. 2010; Fraser-McKelvie et al. 2016) and the presence of large reserves of H I which usually correlates with strong star formation (Saintonge et al. 2012). While some galaxies have central fiber spectra which place them on the star formation sequence of galaxies (Fig. 4), they are all in the quiescent region of the D_n4000 versus $H\delta_A$ plot (Fig. 6), although with a wide range of D_n4000 values, suggesting a wide range of population ages.

Secondly, we find that, as predicted by the simulations of Athanassoula et al. (2013), not all of the HIRB galaxies have a H I ‘hole’ in the centre, where the gas has been driven into the centre or prevented from entering the region due to the strong bar. The simulations show that the time-scale for H I hole formation depends on the gas content, so we explain this as some of the strong bars in the sample are in such gas-rich galaxies that the bar formation has been delayed and they have not had adequate time to funnel all of the gas in the central region.

We observe a correlation between the H I morphology and star formation properties of the galaxy, which are divided into those which have dynamically mature bars, H I holes, and have apparently ceased star formation, and those which are more gas rich, do not

have H I holes (suggesting dynamically younger bars), and are still actively star forming. This does support a picture in which bar quenching play an important role in the evolution of disc galaxies.

Through the resolved H I data we see that four of the HIRB galaxies have nearby companions; not all were obviously interacting from the SDSS optical images. This seemingly high proportion of interactions suggests a close ‘fly-by’ or an impending merger of the galaxies, and this disruption to the secular evolution could have either tidally triggered the formation of the bar, or added H I gas to the galaxy after the bars had formed. This process might offer an explanation as to why those galaxies have formed their bar before they have had a chance to use all of the H I reserves. This role of environment on HIRB galaxy evolution will be investigated further in a future paper (Newnham et al., in preparation).

Galaxy evolution is a complex system in which many physical processes play a role. While the role that bars and other secular processes play in galaxy evolution is not always considered in studies of the general galaxy population, we demonstrate with our HIRB sample that it can be significant in massive spiral galaxies (e.g. including our own Milky Way), and therefore its role in the broader processes of galaxy evolution should not be neglected. Further study with larger samples of strongly barred galaxies with resolved gas and stellar kinematics will be needed to fully understand the significance of this process to the broader galaxy population.

ACKNOWLEDGEMENTS

We thank the staff of the Giant Metrewave Radio Telescope who have made these observations possible. The Giant Metrewave Radio Telescope is run by the National Centre for Radio Astrophysics of the Tata Institute of Fundamental Research. The Karl G. Jansky Very Large Array is operated by The National Radio Astronomy Observatory. AIPS and CASA are produced and managed by The National Radio Astronomy Observatory. The National Radio Astronomy Observatory is a facility of the National Science Foundation operated under cooperative agreement by Associated Universities, Inc. This work makes use of the Arecibo Legacy Fast ALFA survey, based on observations made with the Arecibo Observatory. The Arecibo Observatory is operated by SRI International under a cooperative agreement with the National Science Foundation (AST-1100968), and in alliance with Ana G. Méndez-Universidad Metropolitana, and the Universities Space Research Association. We wish to acknowledge all members of the Arecibo Legacy Fast ALFA team for their work in making Arecibo Legacy Fast ALFA possible. This research has made use of the NASA/IPAC Extragalactic Database, which is operated by the Jet Propulsion Laboratory, California Institute of Technology, under contract with the National Aeronautics and Space Administration. This research has made use of SAOImage DS9, developed by Smithsonian Astrophysical Observatory (<http://hea-www.harvard.edu/RD/ds9/>). Funding for the SLoan Digital Sky Survey and Sloan Digital Sky Survey-II was provided by the Alfred P. Sloan Foundation, the Participating Institutions, the National Science Foundation, the U.S. Department of Energy, the National Aeronautics and Space Administration, the Japanese Monbukagakusho, the Max Planck Society, and the Higher Education Funding Council for England. The Sloan Digital Sky Survey Web Site is <http://www.sdss.org/>. Galaxy Evolution Explorer is a National Aeronautics and Space Agency mission managed by the Jet Propulsion Laboratory. LN acknowledges studentship funding from the Science and Technology Facilities Council ST/N504245/1, and a supplementary Long Term Attachment grant to visit KLM at

Haverford College. LN would like to thank Haverford College for hospitality during her visit (2018 June–2019 May).

REFERENCES

- Abazajian K. N. et al., 2009, *ApJS*, 182, 543
- Athanassoula E., 1992, *MNRAS*, 259, 345
- Athanassoula E., 2002, in Athanassoula E., Bosma A., Muijica R., eds, ASP Conf. Ser. Vol. 275, Discs of Galaxies: Kinematics, Dynamics and Perturbations. Aston. Soc. Pac., San Francisco, p. 141
- Athanassoula E., 2013, Bars and Secular Evolution in Disc Galaxies: Theoretical Input. Cambridge University Press, Cambridge, UK, p. 305
- Athanassoula E., Machado R. E. G., Rodionov S. A., 2013, *MNRAS*, 429, 1949
- Baldwin J. A., Phillips M. M., Terlevich R., 1981, *PASP*, 93, 5
- Barazza F. D., Jogee S., Marinova I., 2008, *ApJ*, 675, 1194
- Berentzen I., Heller C. H., Shlosman I., Fricke K. J., 1998, *MNRAS*, 300, 49
- Bigiel F., Leroy A., Walter F., Brinks E., de Blok W. J. G., Madore B., Thornley M. D., 2008, *AJ*, 136, 2846
- Blanton M. R., Roweis S., 2007, *AJ*, 133, 734
- Blanton M. R. et al., 2005, *AJ*, 129, 2562
- Bottema R., Verheijen M. A. W., 2002, *A&A*, 388, 793
- Bournaud F., Combes F., 2002, *A&A*, 392, 83
- Brinchmann J., Charlot S., White S. D. M., Tremonti C., Kauffmann G., Heckman T., Brinkmann J., 2004, *MNRAS*, 351, 1151
- Carles C., Martel H., Ellison S. L., Kawata D., 2016, *MNRAS*, 463, 1074
- Catinella B., Cortese L., 2015, *MNRAS*, 446, 3526
- Cervantes Sodi B., 2017, *ApJ*, 835, 80
- Chapelon S., Contini T., Davoust E., 1999, *A&A*, 345, 81
- Cheung E. et al., 2013, *ApJ*, 779, 162
- Cheung E. et al., 2015, *MNRAS*, 447, 506
- Combes F., 2008, in Bureau M., Athanassoula E., Barbuy B., eds, Proc. IAU Symp. 245, Formation and Evolution of Galaxy Bulges. Kluwer, Dordrecht, p. 151
- Corwin H. G. Jr, Buta R. J., de Vaucouleurs G., 1994, *AJ*, 108, 2128
- Davoust E., Contini T., 2004, *A&A*, 416, 515
- Ellison S. L., Nair P., Patton D. R., Scudder J. M., Mendel J. T., Simard L., 2011, *MNRAS*, 416, 2182
- Elmegreen B. G., Elmegreen D. M., Chromey F. R., Hasselbacher D. A., Bissell B. A., 1996, *AJ*, 111, 2233
- England M. N., 1989, *ApJ*, 344, 669
- Erwin P., 2005, *MNRAS*, 364, 283
- Erwin P., 2018, *MNRAS*, 474, 5372
- Eskridge P. B. et al., 2000, *AJ*, 119, 536
- Fanali R., Dotti M., Fiacconi D., Haardt F., 2015, *MNRAS*, 454, 3641
- Foreman-Mackey D., Hogg D. W., Lang D., Goodman J., 2013, *PASP*, 125, 306
- Fraser-McKelvie A., Brown M. J. I., Pimblett K. A., Dolley T., Crossett J. P., Bonne N. J., 2016, *MNRAS*, 462, L11
- Galloway M. A. et al., 2015, *MNRAS*, 448, 3442
- Gavazzi G. et al., 2015, *A&A*, 580, A116
- George K., Joseph P., Mondal C., Subramanian S., Subramanian A., Paul K. T., 2018, *A&A*, 621, L4
- Giovanelli R. et al., 2005, *AJ*, 130, 2598
- Giuricin G., Mardirossian F., Mezzetti M., Monaco P., 1993, *ApJ*, 407, 22
- Greisen E. W., 2003, in Heck A., ed., Astrophysics and Space Science Library, Vol. 285, Information Handling in Astronomy – Historical Vistas. Springer-Verlag, Berlin, p. 109
- Hallenbeck G. et al., 2014, *AJ*, 148, 69
- Hart R. E., Bamford S. P., Keel W. C., Kruk S. J., Masters K. L., Simmons B. D., Smethurst R. J., 2018, *MNRAS*, 478, 932
- Haynes M. P. et al., 2011, *AJ*, 142, 170
- Haynes M. P. et al., 2018, *ApJ*, 861, 49
- Haywood M., Lehnert M. D., Di Matteo P., Snaith O., Schultheis M., Katz D., Gómez A., 2016, *A&A*, 589, A66
- Hohl F., 1976, *AJ*, 81, 30
- Hoyle B. et al., 2011, *MNRAS*, 415, 3627
- Huang S. et al., 2012, Old Stars in the Massive, Gas-Rich HighMass Galaxies, Spitzer Proposal
- Hunter J. H. J., 1990, *Ann. New York Acad. Sci.*, 596, 174
- James P. A., Percival S. M., 2016, *MNRAS*, 457, 917
- James P. A., Percival S. M., 2018, *MNRAS*, 474, 3101
- Kauffmann G. et al., 2003, *MNRAS*, 341, 33
- Khoperskov S., Haywood M., Di Matteo P., Lehnert M. D., Combes F., 2018, *A&A*, 609, A60
- Kim E., Hwang H. S., Chung H., Lee G.-H., Park C., Cervantes Sodi B., Kim S. S., 2017, *ApJ*, 845, 93
- Kormendy J., Kennicutt R. C. Jr, 2004, *ARA&A*, 42, 603
- Kraljic K., Bournaud F., Martig M., 2012, *ApJ*, 757, 60
- Kruk S. J. et al., 2018, *MNRAS*, 473, 4731
- Laine S., Gottesman S. T., 1998, *MNRAS*, 297, 1041
- Lee C., Chung A., Yun M. S., Cybulski R., Narayanan G., Erickson N., 2014, *MNRAS*, 441, 1363
- Lemonias J. J., Schiminovich D., Catinella B., Heckman T. M., Moran S. M., 2014, *ApJ*, 790, 27
- Leroy A. K., Walter F., Brinks E., Bigiel F., de Blok W. J. G., Madore B., Thornley M. D., 2008, *AJ*, 136, 2782
- Li C., Gadotti D. A., Mao S., Kauffmann G., 2009, *MNRAS*, 397, 726
- Lin Y., Cervantes Sodi B., Li C., Wang L., Wang E., 2014, *ApJ*, 796, 98
- Lindblad P. A. B., Kristen H., Joersaeter S., Hoegbom J., 1997, *A&A*, 317, 36
- Marinova I. et al., 2012, *ApJ*, 746, 136
- Martel H., Kawata D., Ellison S. L., 2013, *MNRAS*, 431, 2560
- Martin D. C. et al., 2005, *ApJ*, 619, L1
- Martin P., 1995, *AJ*, 109, 2428
- Martinet L., Friedli D., 1997, *A&A*, 323, 363
- Martinez-Valpuesta I., Shlosman I., Heller C., 2006, *ApJ*, 637, 214
- Masters K. L. et al., 2010, *MNRAS*, 405, 783
- Masters K. L. et al., 2011, *MNRAS*, 411, 2026
- Masters K. L. et al., 2012, *MNRAS*, 424, 2180
- McMullin J. P., Waters B., Schiebel D., Young W., Golap K., 2007, in Shaw R. A., Hill F., Bell D. J., eds, ASP Conf. Ser. Vol. 376, Astronomical Data Analysis Software and Systems XVI. Astron. Soc. Pac., San Francisco, p. 127
- Menéndez-Delmestre K., Sheth K., Schinnerer E., Jarrett T. H., Scoville N. Z., 2007, *ApJ*, 657, 790
- Moore E. M., Gottesman S. T., 1998, *MNRAS*, 294, 353
- Moore B., Katz N., Lake G., Dressler A., Oemler A., 1996, *Nature*, 379, 613
- Nair P. B., Abraham R. G., 2010a, *ApJS*, 186, 427
- Nair P. B., Abraham R. G., 2010b, *ApJS*, 714, L260
- Noguchi M., 1988, *A&A*, 203, 259
- Oh S., Oh K., Yi S. K., 2012, *ApJS*, 198, 4
- Ostriker J. P., Peebles P. J. E., 1973, *ApJ*, 186, 467
- Pfenniger D., Norman C., 1990, *ApJ*, 363, 391
- Regan M. W., Sheth K., Vogel S. N., 1999, *ApJ*, 526, 97
- Rozas M., Knapen J. H., Beckman J. E., 1998, *MNRAS*, 301, 631
- Saha K., Elmegreen B., 2018, *ApJ*, 858, 24
- Saintonge A. et al., 2011, *MNRAS*, 415, 61
- Saintonge A. et al., 2012, *ApJ*, 758, 73
- Salim S. et al., 2007, *ApJS*, 173, 267
- Sault R. J., Teuben P., Wright M. C. H., 2011, Astrophysics Source Code Library, record ascl:1106.007
- Schawinski K. et al., 2014, *MNRAS*, 440, 889
- Schaye J., 2004, *ApJ*, 609, 667
- Schwarz M. P., 1984, *MNRAS*, 209, 93
- Sellwood J. A., Shen J., Li Z., 2019, *MNRAS*, 486, 4710
- Serra P. et al., 2015, *MNRAS*, 448, 1922
- Sheth K., Scoville N. Z., Vogel S. N., Aalto S., Huettemeister S., Regan M. W., Das M., 2003, Proc. IAU Symp., Vol. 221, Deciphering Star Formation with the Barred Spiral Laboratory. p. P34
- Sheth K., Vogel S. N., Regan M. W., Thornley M. D., Teuben P. J., 2005, *ApJ*, 632, 217
- Skibba R. A. et al., 2012, *MNRAS*, 423, 1485
- Smethurst R. J. et al., 2015, *MNRAS*, 450, 435

- Spinoso D., Bonoli S., Dotti M., Mayer L., Madau P., Bellovary J., 2017, *MNRAS*, 465, 3729
- Springob C. M., Haynes M. P., Giovanelli R., Kent B. R., 2005, *ApJS*, 160, 149
- Stoughton C. et al., 2002, *AJ*, 123, 485
- Strauss M. A. et al., 2002, *AJ*, 124, 1810
- Tubbs A. D., 1982, *ApJ*, 255, 458
- van den Bergh S., 2002, *AJ*, 124, 782
- Vera M., Alonso S., Coldwell G., 2016, *A&A*, 595, A63
- Villa-Vargas J., Shlosman I., Heller C., 2010, *ApJ*, 719, 1470
- Walter F., Brinks E., de Blok W. J. G., Bigiel F., Kennicutt Robert C. J., Thornley M. D., Leroy A., 2008, *AJ*, 136, 2563
- Wang J. et al., 2013, *MNRAS*, 433, 270
- Weiner B. J., Sellwood J. A., Williams T. B., 2001, *ApJ*, 546, 931
- Willett K. W. et al., 2013, *MNRAS*, 435, 2835

This paper has been typeset from a $\text{\TeX}/\text{\LaTeX}$ file prepared by the author.